frontiers | Frontiers in Imaging

TYPE Review
PUBLISHED 08 January 2026
DOI 10.3389/fimag.2025.1694840

OPEN ACCESS

EDITED BY
Moulay Akhloufi,
Université de Moncton, Canada

REVIEWED BY
Timothy P. Fitzgibbons,
University of Massachusetts Medical School, United States
Se-Hong Kim,
The Catholic University of Korea, Republic of Korea

*CORRESPONDENCE
Julian Rene Cuellar Buritica
✉ jucuell@siue.edu

RECEIVED 28 August 2025
REVISED 24 November 2025
ACCEPTED 04 December 2025
PUBLISHED 08 January 2026

CITATION
Cuellar Buritica JR, Bhattarai M, Carrillo P, Burri M and Klingensmith J (2026) Cardiac adipose tissue, imaging segmentation, and quantification for cardiovascular disease assessment. *Front. Imaging* 4:1694840. doi: 10.3389/fimag.2025.1694840

Cardiac adipose tissue, imaging segmentation, and quantification for cardiovascular disease assessment

Julian Rene Cuellar Buritica[1]*, Mukul Bhattarai[2], Pedro Carrillo[1], Manjula Burri[3] and Jon Klingensmith[1]

[1]Biomedical Imaging Research Lab, Department of Electrical and Computer Engineering, School of Engineering, Southern Illinois University Edwardsville, Edwardsville, IL, United States, [2]School of Medicine, Southern Illinois University, Springfield, IL, United States, [3]Columbus Regional Hospital, Columbus, IN, United States

Cardiac adipose tissue (CAT) has emerged as a critical and clinically relevant factor in cardiovascular disease (CVD), yet its full impact remains largely overlooked. The amount of fat surrounding the heart can influence major blood vessels by promoting plaque formation. In conditions such as cardiac steatosis or fatty heart disease, fat infiltration or accumulation within the heart muscle compromises its function may play a role in heart failure (HF) and coronary artery disease (CAD). This review explores the different types of fat deposits surrounding the heart, focusing on the potential contribution of CAT to cardiovascular disease (CVD). Three main imaging modalities for assessing cardiac fat are discussed, including magnetic resonance imaging (MRI), computed tomography (CT), and echocardiography. The segmentation and quantification of the fat for each imaging modality are also presented, correlating these measurements with CVD risk. Each imaging modality offers distinct advantages and limitations in segmenting and quantifying fat. Despite its clinical significance, quantification and characterization of CAT remain challenging, requiring advanced imaging techniques for precise assessment. Future research should focus on unlocking the mechanistic pathways that link CAT to adverse cardiovascular outcomes, ultimately enhancing our ability to predict, prevent, and treat heart disease with greater precision. As imaging technology advances, there is a need for refined segmentation methods and consensus-driven guidelines to establish CAT as a key biomarker in CVD risk stratification.

KEYWORDS

cardiac adipose tissue, cardiovascular disease, ultrasound, MRI, CT, segmentation, quantification, deep learning

1 Introduction

Adipose tissue (AT), commonly known as body fat, is a specialized form of connective tissue. It is composed of adipocytes or "fat cells" and additional minor cell types such as fibroblasts, endothelial cells, macrophages, stromal cells, immune cells, and pre-adipocytes (Kim et al., 2023). Inside the adipocytes, lipid droplets surrounded by a structural network of fibers perform the energy storage function of these cells, as shown in Figure 1 (Hernandez et al., 2025). AT exists in two major forms: white adipose tissue (WAT), which serves as the primary energy storage depot in the form of triglycerides and secretes adipokines (Farese and Walther, 2009), and brown adipose tissue (BAT), which

is metabolically active and involved in thermogenesis through mitochondrial uncoupling proteins (Sacks and Symonds, 2013). In adults, brown adipose tissue surrounds the vertebrae, is located above the clavicles, is in the upper back, and is in the central compartment of the thoracic cavity. White adipose tissue is composed of white and beige adipocytes and is the most abundant type of fat in humans, including the fat that surrounds the internal body organs called visceral adipose tissue (VAT).

Within the cardiovascular system, most of the AT corresponds to WAT. Distinct fat depots collectively referred to as cardiac adipose tissue (CAT) include epicardial adipose tissue (EAT), pericardial adipose tissue (PAT), and paracardial adipose tissue (PcAT), each differing in anatomical location and physiological impact (Fitzgibbons and Czech, 2014). EAT, located between the myocardium and the visceral pericardium, is the most clinically relevant depot because it shares microcirculation with the myocardium and coronary arteries, allowing direct paracrine and vasocrine interactions. Rather than being a passive energy reservoir, CAT is a metabolically active organ that exerts local and systemic effects through the secretion of adipokines, inflammatory mediators, and bioactive molecules. These factors influence myocardial structure, coronary artery function, and pericardial dynamics, contributing to conditions such as coronary artery disease, atrial fibrillation, and heart failure.

2 Cardiac tissue layers and adipose depots

The tissue layers that enclose each heart's chamber are shown in Figure 2a, starting with the innermost tissue layer (the endocardium), and extending outward to the paracardial fat (Gaborit et al., 2017). A basic classification of the adipose tissue around the heart consists of the epicardial adipose tissue (EAT) and the pericardial adipose tissue (PAT); together, these two layers form the cardiac adipose tissue (CAT), where the visceral pericardium is the layer between them, as shown in Figure 2b (Iacobellis, 2015; Cheładze et al., 2022; Konwerski et al., 2022). This classification considers the EAT and PAT, but also includes the paracardial adipose tissue (PcAT) and perivascular adipose tissue (PvAT).

2.1 Epicardial adipose tissue

The epicardial adipose tissue (EAT) is located beneath the visceral pericardium and has anatomical, histological, embryonic, and genetic differences from other types of fat (Gaborit et al., 2017; Iacobellis, 2015). EAT does not have fascia separating it from the vessels and myocardium. This allows both paracrine and vasocrine effects via adipokines, cytokines, and chemokines (Gaborit et al., 2017; Mazurek et al., 2003). It is vascularized by the coronary circulation, and its cellular composition primarily consists of white adipocytes, with some beige and brown adipocyte concentrations (Chhabra and Gurukripa Kowlgi, 2015; Krauz et al., 2024). On average, the EAT corresponds to 20% of the total heart weight, but its amount and distribution vary from 4% to 52% among individuals. EAT depots are found mainly over the base of the heart, the left ventricular apex, the atrioventricular and interventricular grooves, around the coronary arteries and veins, and over the right ventricle, especially the free wall of the right ventricle (Silaghi et al., 2008). Several mechanisms of the EAT are linked to its contribution to CVD, including its proinflammatory profile, the release of different reactive oxygen species (ROS), and fatty infiltration into the atria and ventricles (Rhee et al., 2017; Gaeta et al., 2017; Zhou et al., 2020). However, direct metabolic assessment of EAT and its precise role in CVD remains challenging. Instead, studies have associated EAT thickness (>6.2 mm) and volume (>101.2 cm^3) with major cardiovascular conditions such as coronary artery disease (CAD), heart failure (HF), and atrial fibrillation (AF; Iacobellis, 2015, 2022; Mahmoud et al., 2021; Abdulkareem et al., 2022). Other studies have investigated the role of EAT and atherosclerotic plaque development and rupture (Song et al., 2023; Van Woerden et al., 2022; Si et al., 2023).

2.2 Pericardial adipose tissue

Pericardial adipose tissue (PAT) is located over the parietal and fibrous pericardium layers and is also referred to as paracardial adipose tissue (Chhabra and Gurukripa Kowlgi, 2015; Iacobellis, 2009). In some literature, PAT is combined with EAT for quantification and correlation with heart disease (Gaborit et al., 2017; Ding et al., 2008). PAT is separated physically from the myocardium by a layer of visceral pericardium as shown in Figures 2a, b. It receives blood supply from non-coronary arteries such as the pericardiophrenic artery, musculophrenic artery, and some branches of the bronchial and esophageal arteries (Drake et al., 2014; Stauffer et al., 2024). Studies have linked PAT to body mass index (BMI), visceral fat, triglycerides, and CAD (Ding et al., 2008; Sicari et al., 2011).

2.3 Paracardial adipose tissue

The paracardial adipose tissue (PcAT) is located outside the parietal and fibrous pericardium (Gaborit et al., 2017) on its external surface (Yamaguchi et al., 2015), within the thoracic cavity but external to the pericardial sac. This positioning means PcAT is separated from the coronary arteries by the pericardial layers, unlike epicardial adipose tissue (EAT) and pericoronary adipose tissue (PCAT), which are in direct contact with the myocardium and coronary vessels. Imaging studies using computed tomography and magnetic resonance consistently describe the pericardium as the anatomical boundary between EAT and PcAT, with PcAT appearing external to this boundary (Demmert et al., 2025). In some literature, this fat depot is called mediastinal fat or intrathoracic fat (Mahabadi et al., 2009), but it can also include the PAT (Rodrigues et al., 2022). Because PcAT lacks direct anatomical continuity with the coronary vasculature, its influence on coronary artery disease (CAD) is considered more systemic rather than local. Reviews emphasize that PcAT influences cardiovascular health indirectly through systemic inflammatory and metabolic pathways (Fitzgibbons and Czech, 2014). Its volume is typically assessed using multi-detector computed tomography (MDCT) by subtracting PAT volume from total thoracic fat, as illustrated in Figure 3.

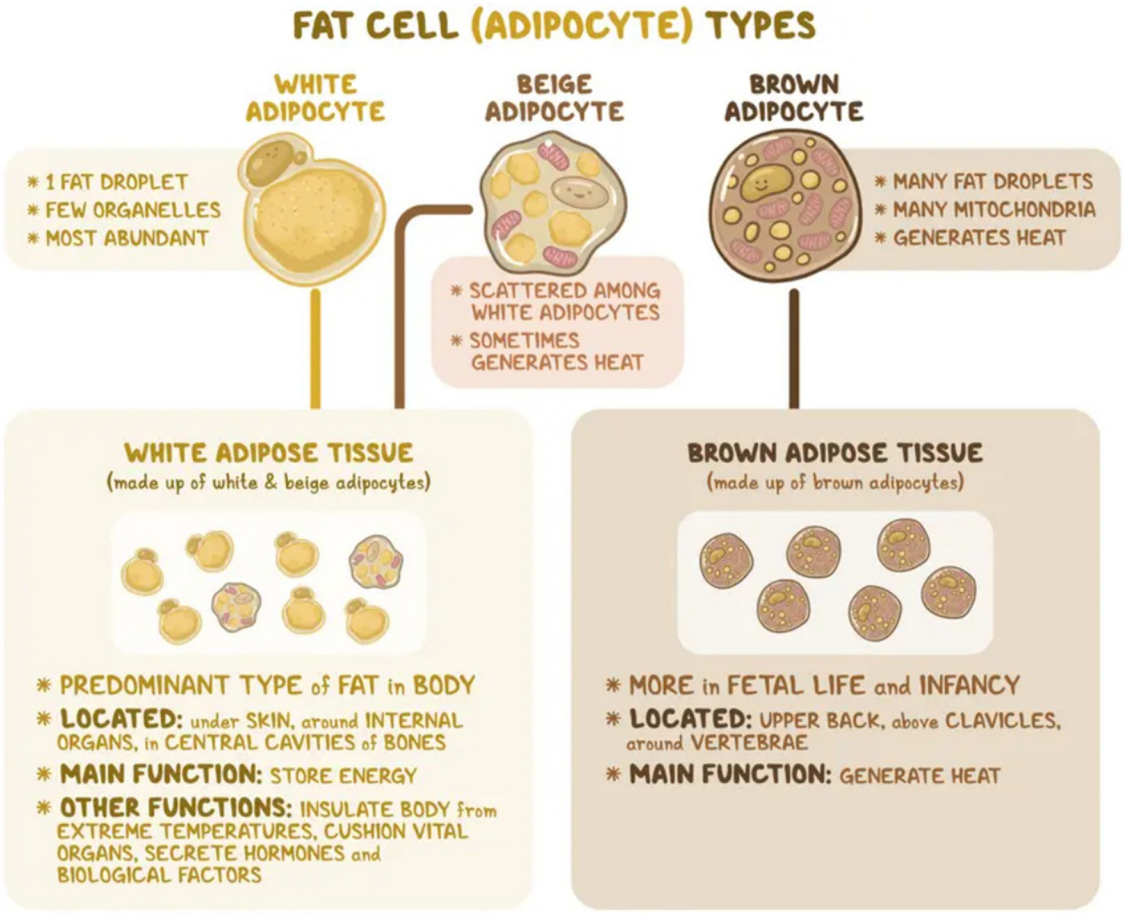

FIGURE 1
Types of adipocytes (Hernandez et al., 2025).

2.4 Perivascular adipose tissue

Perivascular adipose tissue (PvAT) surrounds adventitia of blood vessels, including the coronary arteries and the aorta, where it is specifically referred to as periaortic adipose tissue (PaAT; Gaborit et al., 2017; Zhang P. et al., 2020; Figure 2b). The PaAT has an average thickness of 3.34 ± 0.79 mm, while the mean aorta wall thickness is 2.38 ± 0.79 mm. An important characteristic of the PaAT is its distribution, which presents a regular pattern around the aorta (Alkhalil et al., 2018). A notable subtype of PvAT is peri-coronary AT (PCAT), which surrounds the coronary arteries (Figures 2c, d). PvAT contributes to less than 0.3% of the total human body adipose tissue (Grigoras et al., 2019). PvAT cellular composition is characterized by adipocytes and inflammatory cells; it also includes microvascular supply and nerve fiber structures, as illustrated in Figure 2e. Its composition varies by location—for instance, periaortic AT in the thoracic region contains brown adipocytes, whereas periaortic AT in the abdominal region consists primarily of white adipocytes (Tran et al., 2018; van Dam et al., 2017). Dysfunctional PvAT has been implicated in obesity-related hypertension, atherosclerotic plaque formation, ischemic coronary artery disease development, atheromatous plaque formation, and reduced vascular protective properties due to its production of pro-inflammatory substances (Virdis et al., 2015; Withers et al., 2014). Radiomics features extracted from PCAT, when combined with clinical variables, have shown improved performance in predicting ischemia and coronary atherosclerosis (Militello et al., 2023). Additional studies have explored the use of PCAT radiomics for evaluating ischemic stenosis, comparing vessel-based and lesion-based segmentation approaches. However, these analyses revealed no significant differences in the diagnosis accuracy between the two methods (Wen et al., 2022). Beyond the coronary context, PvAT has also been investigated using CT imaging. One study demonstrated a correlation between alterations in PvAT density and the presence of abdominal aortic aneurysms, suggesting its potential role as an imaging biomarker for vascular disease (Ginzburg et al., 2024).

3 Cardiac fat and cardiovascular disease (CVD)

3.1 Coronary artery disease (CAD)

Coronary artery disease (CAD) results in a deficient supply of oxygenated blood to the heart muscle due to the buildup of

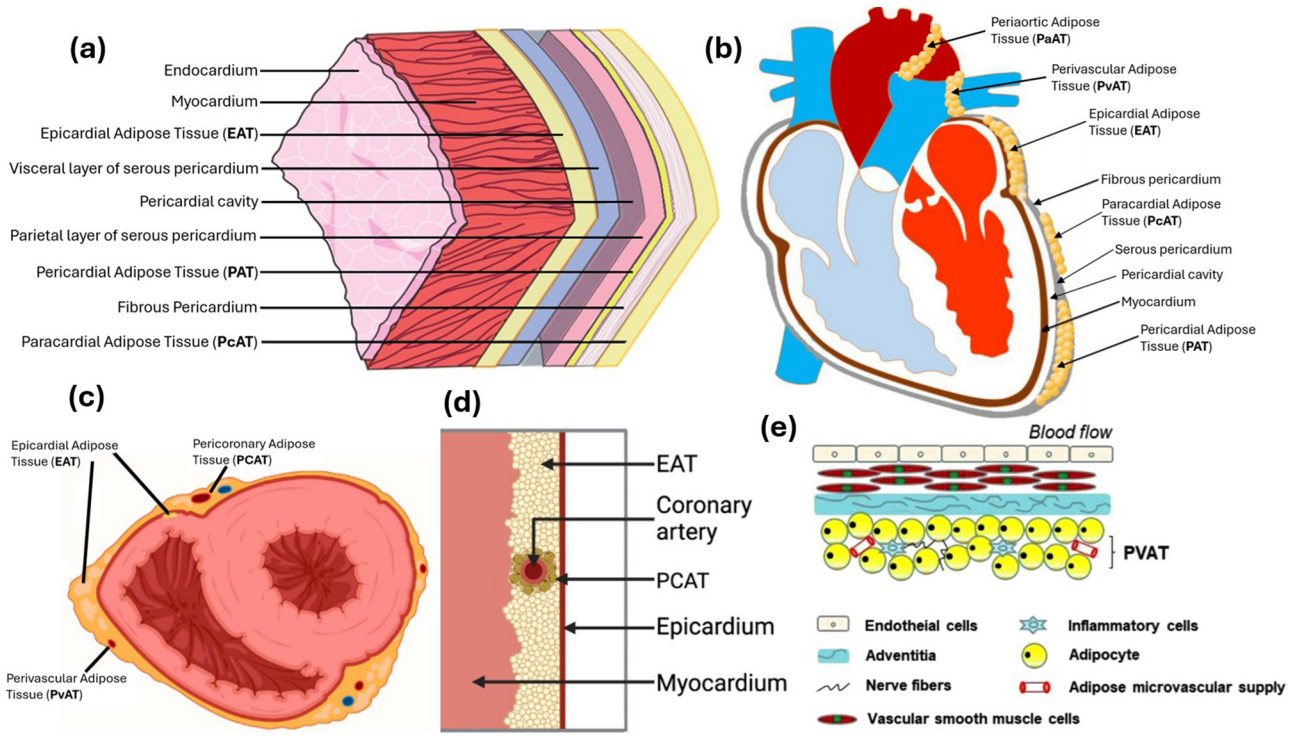

FIGURE 2
Heart wall tissue layers and classification of cardiac fat. **(a)** Tissue layers on the heart's walls (Gaborit et al., 2017), **(b)** common classification of fat around the heart (Kim et al., 2023; Iacobellis, 2015; Konwerski et al., 2022), **(c)** perivascular AT (PvAT) and pericoronary AT (PCAT), **(d)** PCAT detail (Krauz et al., 2024), and **(e)** PvAT composition (Zhang P. et al., 2020).

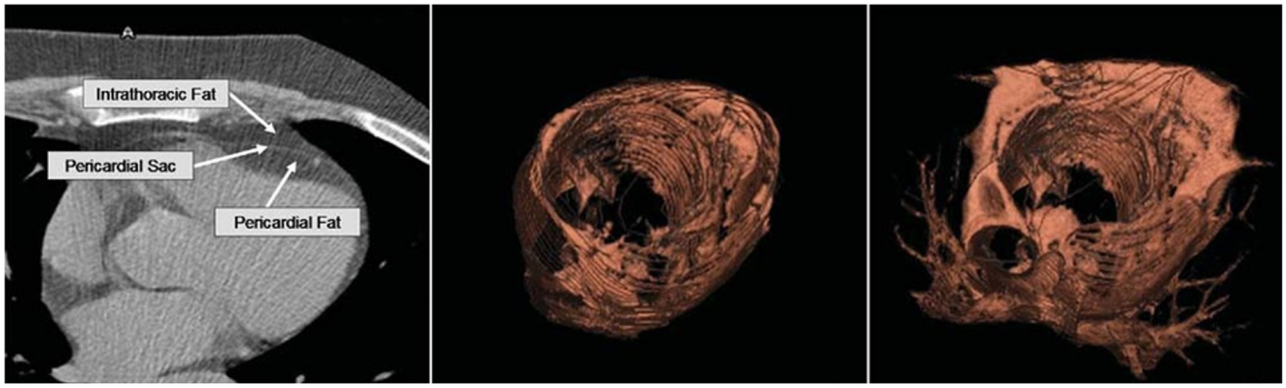

FIGURE 3
PcAT identified as intrathoracic fat and 3D reconstructions of PAT and PcAT (Mahabadi et al., 2009).

atherosclerotic plaques (cholesterol deposits) inside the arteries, causing narrowing and obstruction (Cleveland Clinic, 2023; Mayo Clinic, 2024a). CAD is also referred to as coronary heart disease (CHD) or coronary stenosis (Mancio et al., 2018). As shown in Figure 4a, an obstructive plaque can trigger blood clot formation, further reducing arterial blood flow. In Figure 4b, illustrates the progression of plaque development, including plaque growth, arterial wall damage, and eventual rupture. The lack of treatment for CAD could lead to angina (chest pain and shortness of breath), heart attack (complete artery blockage due to a clot), HF, and arrhythmias. Studies using CT scans have identified PAT volumes exceeding 300 cm^3 as a reliable predictor of CAD, comparable with the Framingham Risk Score (Mahabadi et al., 2009; Ding et al., 2009). In studies using CT scans and echocardiography, it was found that the EAT thickness at the left atrioventricular groove was the best predictor for obstructive CAD (Wu et al., 2013; Hirata et al., 2015). In healthy/asymptomatic subjects, a study demonstrated that an EAT thickness larger than 2.4 mm is a predictor of coronary stenosis exceeding 50% occlusion as determined by multidetector computed tomography (MDCT; Bachar et al., 2012).

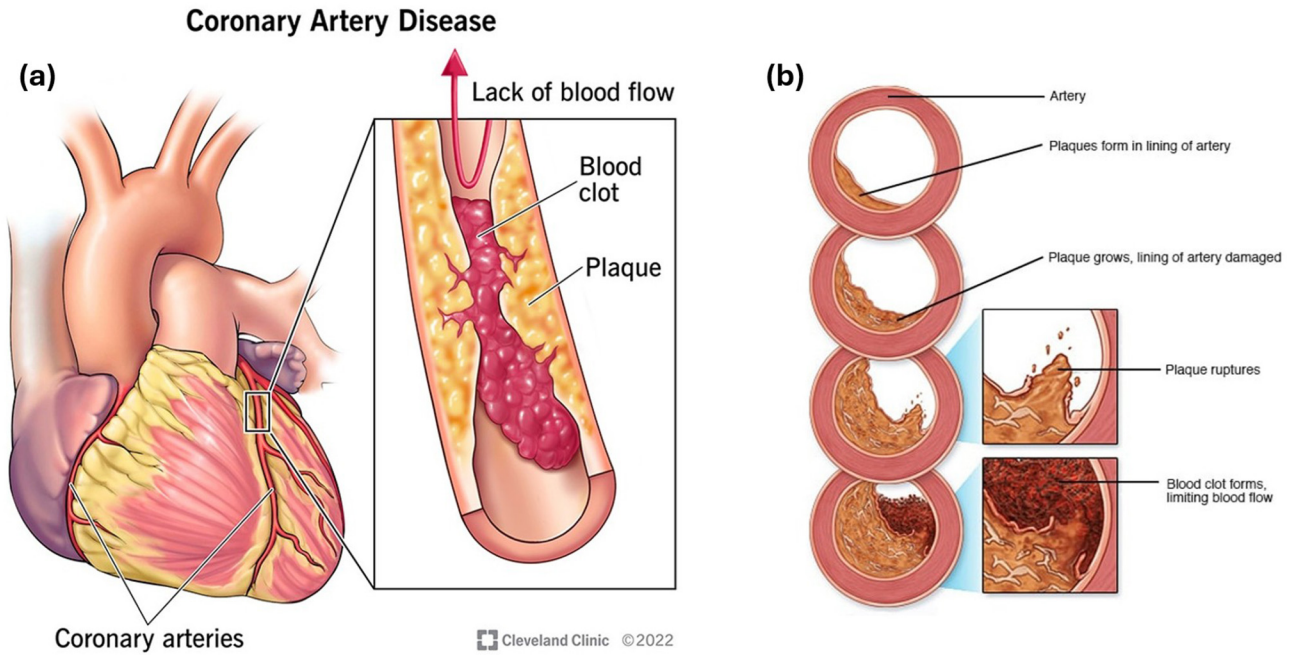

FIGURE 4
Coronary artery disease. **(a)** Coronary arteries and obstructive plaque (Cleveland Clinic, 2023) and **(b)** plaque development (Mayo Clinic, 2024a).

3.2 Heart failure (HF)

Heart failure (HF), also known as congestive heart failure (CHF), is a chronic condition that develops when the heart muscle is unable to pump blood effectively throughout the body. This impaired pumping function can be caused by various factors that weaken or stiffen the heart muscle, ultimately leading to a shortage of oxygen-rich blood reaching vital organs (Mayo Clinic, 2025b). Heart failure is classified based on ejection fraction (EF)—the percentage of blood ejected from the left ventricle per heartbeat. HF is categorized as: HF with reduced EF (<40%, HFrEF), with mildly reduced EF (41%−49%), and HF with preserved EF (>50%, HFpEF; Malik et al., 2024). The relationship between EAT and HF remains an area of active research. Some studies demonstrated that increased EAT volume may have a protective role in HFrEF (Pugliese et al., 2021), while in HFpEF, excess EAT is associated with adverse cardiometabolic effects (Tromp et al., 2021). EAT expansion and inflammation promote diastolic dysfunction through mechanical restraint that limits ventricular compliance, secretion of pro-inflammatory cytokines and adipokines that drive myocardial fibrosis and endothelial dysfunction, and lipotoxicity that exacerbates oxidative stress and metabolic derangements (Qi et al., 2025; Menghoum et al., 2025). These mechanisms collectively reproduce the HFpEF phenotype characterized by elevated filling pressures, systemic inflammation, and exercise intolerance, even in non-obese individuals. Furthermore, EAT density and inflammatory profile have been associated with adverse outcomes and are being explored as therapeutic targets, with interventions such as caloric restriction (Iacobellis and Willens, 2009). Conversely, in HFrEF, some evidence suggests EAT may provide local energy substrates and exert a protective role during advanced systolic dysfunction (Pugliese et al., 2021), highlighting the complex and phenotype-specific role of EAT in heart failure.

3.3 Atrial fibrillation

Atrial fibrillation (AF) is a common cardiac arrhythmia that disrupts the heart's natural electrical conduction. In a healthy heart, the sinoatrial (SA) node acts as the pacemaker, generating electrical impulses in a coordinated contraction of the heart muscle. These impulses propagate through the atria, causing their contraction and pumping blood into the ventricles. The ventricles then depolarize and contract to circulate the blood throughout the body (Li et al., 2023). However, in AF, the electrical activity within the atria becomes chaotic and disorganized, disrupting the normal contraction pattern. Consequently, the ventricles may not receive these signals consistently, resulting in an irregular and often faster heart rate. AF also causes the enlargement of the left atrium and increased pressure within the atrium (Large et al., 1997; Schneider et al., 2010). Several factors contribute to the development of AF, including hypertension, CAD, valvular heart disease, sleep apnea, obesity, and excessive alcohol consumption (Gaborit et al., 2017; Schneider et al., 2010). Studies using CT scans have shown that epicardial adipose tissue (EAT) around the atria plays a role in AF recurrence (Tsao et al., 2011; Nakanishi et al., 2012; Nagashima et al., 2011).

3.4 Ischemic heart disease

Ischemic heart disease is a group of syndromes caused by myocardial ischemia, which occurs when blood flow to the myocardium is restricted. This imbalance between blood supply and demand deprives the cardiac tissue of the oxygen and nutrients essential for normal function (Steenbergen and Frangogiannis, 2012). The most prevalent cause of myocardial ischemia is CAD,

followed by coronary artery spasm (CAS). CAS is a transient constriction of the coronary arteries that can reduce blood flow and trigger ischemic events (Gul et al., 2024). Studies using non-contrast CT assessed PAT and EAT volumes and found that larger amounts, with concentrations above 96 ± 36 cm^3 for EAT and above 99 ± 4 cm^3 for PAT, are strongly correlated with myocardial ischemia (Tamarappoo et al., 2010; Hell et al., 2016b).

3.5 Heart valve stenosis

Stenosis refers to the narrowing of the diameter of a passage, conduit, or tube in the body. Stenosis can affect the aortic, mitral, tricuspid, or pulmonary valve, making blood flow more (Mayo Clinic, 2024b). The most common cause of valve stenosis is the accumulation of calcium or other mineral deposits and fat residues over the valve leaflets. Excess EAT, particularly when its thickness > 7 mm, has been linked to mitral annular calcification and aortic valve stenosis (Mahabadi et al., 2017; Nabati et al., 2019). Valve stenosis is uncommon in young individuals; however, studies suggest that approximately 2% of people over 65 years old in the United States have some degree of aortic valve stenosis. If left untreated, mitral and aortic valve stenosis can lead to HF, stroke, irregular heart rhythms, and death (Mayo Clinic, 2025a).

3.6 Cardiac steatosis

Cardiac steatosis, also known as myocardial steatosis, lipomatosis cordis, or fatty heart disease, refers to the abnormal accumulation of fat within the heart muscle. The excess fat plays a significant role in diabetic cardiomyopathy, ventricular dysfunction, and end-organ damage (Liu et al., 2010). The infiltrative-lipotoxic and pericardial restraint hypotheses have been postulated as the potential mechanisms that relate EAT to cardiac steatosis (Van Woerden et al., 2022). (1) Infiltrative-lipotoxic hypothesis—EAT infiltrates the myocardium, releasing pro-inflammatory adipokines that impair heart function. (2) Pericardial restraint hypothesis—Excessive EAT accumulation mechanically restricts myocardial expansion, leading to diastolic dysfunction (Figure 5). Myocardial steatosis is a common condition, affecting up to 30% of the population. In severe cases, it can lead to symptoms like fatigue, shortness of breath, chest pain, heart failure, or arrhythmias, with a strong correlation to left ventricular dysfunction (Wu et al., 2020).

3.7 Cardiac fibrosis

Cardiac fibrosis is characterized by the excessive deposition of stiff and inflexible scar tissue in the myocardium that reduces the heart's ability to pump blood effectively (Schimmel et al., 2022). The main cause of cardiac fibrosis is related to heart injuries from heart attacks, hypertension, or diabetes, but the amount of EAT has also been linked with myocardial fibrosis. EAT volume measured using cardiac magnetic resonance (CMR) imaging has demonstrated a strong correlation between EAT volume and myocardial fibrosis, independent of traditional risk factors such as age, hypertension, diabetes, or other HF causes (Wu et al., 2017).

3.8 Cardiac lipoma

Cardiac lipoma is a non-common degenerative process in which myocardial cells are replaced with fat. It is a benign tumor made up of mature fat cells (Ismail et al., 2015). This process primarily affects the myocardial structures, the right atrium, and can originate from the papillary muscle (Radswiki, 2025). Cardiac lipomas are correlated with heart arrhythmias, syncope, palpitations, and angina. Another form of cardiac lipoma is epicardial lipomatosis, sometimes called epicardial lipomatous hypertrophy (ELH). This lipoma involves an excess of non-encapsulated fatty tissue in the epicardium (Weerakkody, 2021). EAT thickness above 20 mm has been linked to ELH, diastolic dysfunction, and tamponade in clinical case reports (Myerson et al., 2004; Miller and Schmitt, 2011). When affecting the interatrial septum, the infiltration of fatty tissue leads to the development of lipomatous hypertrophy of the interatrial septum. This uncommon disorder is associated with arrhythmias, syncope, and sudden death (Gaillard, 2025).

4 Imaging modalities to assess CAT

Accurate assessment of pericardial adipose tissue (PAT) and epicardial adipose tissue (EAT) is crucial for evaluating cardiovascular risk. This process involves segmentation and quantification. Segmentation refers to manual, semi-automatic, and automatic EAT and PAT region identification in medical images. Quantification refers to the measurement of EAT and PAT volume and thickness. This section explores various imaging modalities employed for segmenting and quantifying cardiac fat. Magnetic resonance imaging (MRI) offers exceptional soft tissue contrast and differentiates fat types (Antonopoulos and Antoniades, 2018). However, factors like cost, time, and patient suitability can limit its use (Cheładze et al., 2022). Cardiac computed tomography (cardiac CT) provides a fast and readily available option for EAT measurement, though it involves ionizing radiation (Marwan et al., 2019). Echocardiography, a widely accessible and safe technique, offers estimates of EAT thickness, but with limitations in fat type distinction and visceral fat measurement (Iacobellis and Willens, 2009). This section investigates the advantages, disadvantages, and clinical considerations for each modality to guide the selection of the most appropriate method for individual-specific patient needs.

4.1 Assessment metrics

Evaluation metrics are needed to assess the accuracy of segmentation and quantification compared to expert tracing. First, Dice Similarity Coefficient (DSC) is a popular and effective tool to gauge the similarity of two data sets. It compares the overlap between the ground truth and the predicted segmentation. Values range between 0.0 (no overlap) and 1.0 (perfect overlap; Cuellar

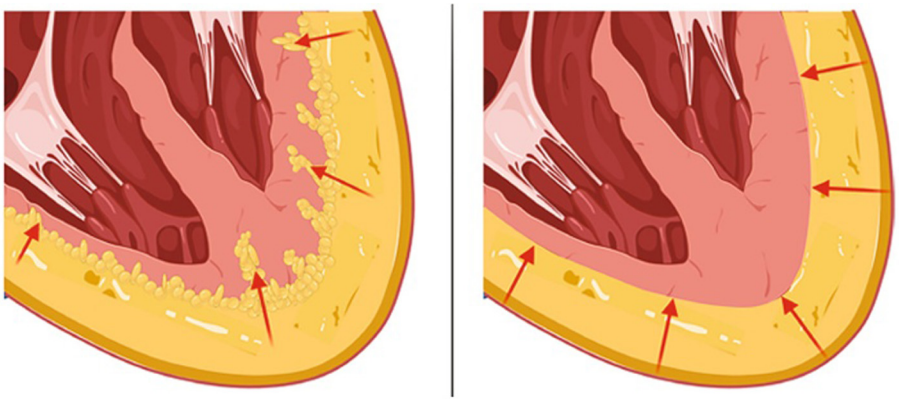

FIGURE 5
Cardiac steatosis by infiltration **(left)**, and by pericardial restraint **(right)** (Van Woerden et al., 2022).

et al., 2025). Next, accuracy is a measure used to evaluate the overall performance of a classification model. Accuracy is the proportion of correct predictions (both true positives and true negatives) out of the total number of predictions made. Similarly, precision, sensitivity, and specificity are comparison metrics used to measure classification performance.

- Precision—The proportion of true positive predictions among all positive predictions made.
- Sensitivity—The proportion of actual positives correctly identified (true positive rate).
- Specificity—The proportion of actual negatives correctly identified (true negative rate).
- F1-score—The harmonic mean of precision and recall, particularly useful for imbalanced datasets.

All four metrics, like DSC, range from 0.0 to 1.0, where values close to 1.0 are considered better segmentation performance. These metrics are commonly used in medical applications to measure the performance of segmentation and quantification efforts. These are among the most common metrics in the given literature used for comparison of different segmentation and quantification methods, as outlined in Tables 1–6.

4.2 Cardiac magnetic resonance (CMR)

MRI utilizes powerful magnetic fields and radio waves to generate high-resolution images of anatomical structures. Cardiac magnetic resonance (CMR) imaging provides excellent soft tissue contrast, enabling detailed visualization of cardiac structures and adipose tissue. Additionally, CMR assesses myocardial fibrosis and myocardial perfusion, providing a comprehensive evaluation of cardiac health (Pohost, 2008). This non-invasive and radiation-free modality delivers high spatial and temporal resolution, effectively distinguishing visceral and parietal layers of the pericardium as shown in Figure 6 (Guglielmo et al., 2021).

4.2.1 Imaging techniques

Novel MRI acquisition strategies have enabled high-resolution, rapid imaging that enhances diagnostic accuracy and provides clearer insights into cardiac structures (Salerno et al., 2017).

Cine MRI is a real-time imaging technique that captures cardiac motion and creates a 3D video. Cine MRI uses steady-state free precession sequencing to acquire a series of slices of the heart in 2-, 3-, and 4-chamber views (Ahmed et al., 2013). Images are then fused to form a cine loop, which visualizes the complete cardiac cycle. Cine imaging provides detailed anatomical information about the heart (Curtis and Cheng, 2022), which helps assess CAT volume and distribution around the beating heart.

The Dixon technique is considered the benchmark for assessing visceral adipose tissue (Homsi et al., 2016). This specific pulse sequence helps separate water and fat signals and relies on the chemical shift difference between water and fat protons. Water and fat have different resonant frequencies in a magnetic field, and this shift enhances the ability to characterize and quantify the two tissues. The Dixon technique can generate water-only and fat-only images, improving the accuracy of EAT quantification.

Gradient echo sequencing provides high spatial resolution and is sensitive to tissue property changes. This imaging technique utilizes gradients to create images exploiting magnetic property differences in different tissue types. The relatively high resolution is beneficial to visualize the thin layers of CAT and distinguish it from adjacent structures like the pericardium. Gradient echo scans can also be combined with other imaging strategies, like the Dixon sequence, to improve tissue separation and enhance visualization of CAT.

4.2.2 CAT segmentation

The segmentation of CAT is particularly challenging compared to other cardiovascular segmentation tasks. CAT's shape is irregular and unevenly distributed, making it hard to detect automatically. Additionally, MRI partial volume effects can blur the pericardium (Militello et al., 2019), leading to mislabeling of CAT as epicardial or paracardial fat due to their similar intensities. Experts visually

TABLE 1 Summary of CAT segmentation studies using MRI.

References	Tissue	Study	Metrics	Values
Feng et al. (2024)	EAT	Automatic double Res-Unet CNN based on fat maps, Dixon MRI	DSC	0.8630
Chen et al. (2023)	PAT	Automatic triple-stage 3SUnet, 2D SA MRI	Precision Recall	0.766 ± 0.152 0.831 ± 0.126
Daudé et al. (2022)	PAT EAT	Automatic four-chamber FCNs, cine MRI	DSC MSD (mm) DSC MSD (mm)	0.7700 1.71 0.8000 2.38
Kulasekara et al. (2022)	CAT	Automatic 3D U-Net, cine MRI	DSC	0.7170
Fulton et al. (2020)	EAT	Automatic double NN, cine MRI	DSC	0.56 ± 0.12

SA, short axis; MSD, mean surface distance; NN, neural network.

TABLE 2 Summary of CAT quantification studies using cardiac MRI.

References	Tissue	Study	Units	Values	Correlation
Guglielmo et al. (2024)	EAT	Automated deep learning volume measurement	mL	43.5 ± 9.0	$p < 0.001$
Secchi et al. (2022)	EAT	Manual volume measurement using open-bore MR, cine MRI	Systole cm^3 Diastole cm^3	88.25 87.00	$p < 0.124$ $p < 0.551$
Henningsson et al. (2020)	EAT	Manual volume measurement using the cine Dixon technique, 3D Dixon MRI	mL	145 ± 90	$p < 0.01$

identified and traced the outline of epicardial fat on each cross-sectional image of the heart (Malavazos et al., 2010). However, this method was labor-intensive, time-consuming, and subject to inter- and intra-observer variability.

To overcome these limitations, machine learning (ML) and deep learning (DL) algorithms have recently automated the segmentation process by finding patterns in the medical images (Karlapalem et al., 2019) or using specific features. ML models are statistical models that map input features into output classes. DL extends the concepts of ML. DL models learn the patterns from the training data. Convolutional neural networks (CNNs) are leveraged to perform tasks to recognize image features. These models produce high accuracy and consistency, can rapidly process large volumes of data, and improve with more training data. This approach, however, requires large, annotated datasets for training, high computational costs, and personnel with expertise in ML/DL. Figure 7 below shows the qualitative results of various DL models compared to manual tracings.

Manual tracings act as the ground truth to assess model prediction accuracy. Table 1 below compares the performance of several ML methods used for CAT segmentation from MRI.

4.2.3 CAT quantification

Much research shows that increased EAT volume is strongly linked to CAD (Song et al., 2023). Therefore, quantifying CAT is necessary for risk assessment and early identification of CAD and other CVDs. CAT volume is calculated by summing the segmented areas across all image slices and multiplying by the slice thickness and pixel dimensions. This method accurately measures the total CAT volume and accounts for the entire heart, calculating fat volume from the base to the apex. This approach, often referred to as the modified Simpson's method, is considered the gold standard for CAT measurement (Requena-Ibáñez et al., 2022). Furthermore, to obtain CAT mass, the fat volume can be simply multiplied by the specific fat density (0.92 g/cm^3). Typically, this approach is done semi-automatically. Experts trace the CAT contours, and a software package is leveraged to sum the areas across all images, taking into account slice thickness and intersection gaps (Henningsson et al., 2020). However, these measurements are time-consuming and cannot be easily incorporated into clinical routine assessments. Recent DL efforts have been employed to automatically quantify CAT. For example, a DL network was developed to automatically quantify EAT on short-axis cine CMR images (Guglielmo et al., 2024). Also, a novel model called PAT-CNN was developed to automate the segmentation and quantification of pericardial adipose tissue from T2-weighted CMR scans (Li et al., 2022). However, manual tracings are still required to validate the performance of such networks. Table 2 compares manual and automatic approaches for CAT quantification in CMR.

4.2.4 Limitations

CAT segmentation and quantification remain complex tasks, even with DL advancements. While DL techniques and methods help mitigate challenges in CMR imaging and improve tissue and EAT visualization, MRI remains an expensive and exclusive imaging modality. It is a high-cost, resource-intensive modality requiring specialized equipment, trained personnel, and extended scan times. Additionally, not all medical centers offer cardiac MRI, limiting accessibility. Patient compliance is another challenge, as MRI requires individuals to remain still for an extended period,

TABLE 3 Summary of CAT segmentation studies using CT.

References	Tissue	Study	Metrics	Values	Correlation
Zhang Q. et al. (2020)	EAT	Automatic dual U-Nets, CT	DSC	0.9119	0.9304
He et al. (2020)	EAT	Automatic 3D deep attention U-Net, CCTA	DSC Precision Recall	0.8550 0.8640 0.8950	NA
Militello et al. (2019)	EAT	Semi-automatic image analysis, CS and CCTA	DSC MAD	0.9374, 0.9248 2.18, 2.87	(Pearson) 0.9591 0.9513
Priya and Sudha (2019)	EAT PAT	Adaptive Region Growing Algorithm, NC CT	Accuracy DSC Accuracy DSC	0.9850 0.9870 0.9640 0.9530	NA
Norlén et al. (2016)		Automatic supervised, CCTA	DSC	0.9900	0.9900
Rodrigues et al. (2016)	EAT PAT	Automatic supervised, CT	DSC Accuracy	0.9810 0.9850	NA

NC, non-contrast; CS, calcium score; CCTA, coronary CT angiography; MAD, mean absolute distance.

TABLE 4 Summary of CAT quantification studies using CT.

References	Tissue	Study	Units	Values	Correlation
Hoori et al. (2022)	EATv	Automatic DeepFat, NC low-dose CS CT	cm^3	100.2 138.6	$R = 0.9833$ $R = 0.9852$
Abdulkareem et al. (2022)	EATv	Automatic single multi-task framework, ECG-gated CT	mL	101.16 103.29	$R = 0.9540$ $R = 0.9430$
Commandeur et al. (2019)	EATv	Automatic CNN, NC CS CT	cm^3	86.75 85.57	$R = 0.9740$ $p < 0.001$
Commandeur et al. (2018)	EATv TATv	Automatic dual ConvNet, NC CCTA	cm^3	130.35 130.94	$R = 0.945$ $p < 0.001$
D'Errico et al. (2017)	T–EATv RV–EATv LV–EATv	Manual volume analysis, NC CCTA	cm^3	103.62, 94.96 67.23, 57.41 38.01, 35.27	ICC = 0.9900

EATv, EAT volume; T-EAT, total EAT; TAT, thoracic adipose tissue; NC, non-contrast; CCTA, coronary CT angiography; CS, calcium score; ICC, intra class correlation.

posing difficulties for those with claustrophobia or severe anxiety. Furthermore, patients with pacemakers or certain metallic implants are ineligible for MRI, further restricting its use. Despite these challenges, MRI remains a desirable modality. With ongoing research and technological advancements, it has the potential to become the preferred method for CAT assessment, improving cardiovascular risk evaluation and clinical decision-making.

4.3 Computed tomography (CT scan)

CT is a powerful imaging modality that uses X-rays to create detailed cross-sectional images of the body. Advanced algorithms combine multiple X-ray measurements from different angles around the patient to reconstruct a 3D representation of the desired anatomy, providing a comprehensive view of the body's internal structures. CT has demonstrated its feasibility and reproducibility for segmenting and quantifying EAT (Tamarappoo et al., 2010). By generating 3D images, CT enables accurate assessment of CAT distribution and precise quantification of CAT volume by measuring attenuation values of fat in Hounsfield Units (HU). Moreover, specialized cardiac CT scans like Coronary CT Angiography (CCTA) and Coronary Artery Calcium (CAC) scoring further enhance characterization of CAT, as shown in Figure 8. Recently, photon-counting CT (PCCT) has emerged as an advanced technology offering improved spatial and contrast resolution compared to conventional CT (Meloni et al., 2023). PCCT scanners convert X-ray photons into electrical signals that are counted and categorized by energy level, resulting in superior image quality and significantly reduced radiation exposure. Research has shown PCCT outperforming conventional CT for the quantification of CAC and significant visual reduction of artifacts on coronary calcified plaques (Flohr et al., 2023). Lastly, CT is considered superior when compared to other imaging modalities for segmenting CAT (Benčević et al., 2022). Unlike MRI, CT does not suffer from pericardial blurring, which is beneficial in distinguishing different adipose tissues. This makes CT the preferred choice in the segmentation and quantification of CAT (Greco et al., 2022).

4.3.1 Imaging techniques

Contrast and non-contrast enhanced CT are the two main primary types of cardiac CT scans used to evaluate adipose tissue and other cardiac structures. Contrast-enhanced CT involves

TABLE 5 Summary of CAT quantification studies using US.

References	Tissue	Study	Units	Values	Correlation
Average from meta-analysis in Wang et al. (2022)	EAT	Meta-analysis of EAT in patients with CAD and Non-CAD groups	mm	5.68 avg 3.61 avg	NA
Eren et al. (2021)	EAT	EAT for atrial fibrillation prediction univariate, multivariate regression ROC EAT > 6.5 mm	mm mm Sensitivity Specificity	8.300, 6.100 5.850, 3.521 0.720 0.770	$p < 0.001$
Xiao et al. (2020)	EAT	EAT thickness and heart disease (control) Coronary heart disease Single-vessel disease Double vessel disease Multi-vessel disease	mm	4.88 6.51 5.66 6.24 6.86	$p < 0.01$ vs. control group
Parisi et al. (2020)	EAT	Validation of EAT thickness assessment for predicting CAD	mm	11.00 (median) 1.00 mm (min) 29.00 mm (max)	$p < 0.001$
Meenakshi et al. (2016)	EAT	EAT thickness as CAD marker	mm	0.9 min 13.5 max 5.56 avg. (men) 5.97 avg. (women)	p (CAD) = 0.0001 p (BMI) = 0.08
Iacobellis et al. (2003)	RV—EAT	Epicardial fat from echocardiography, thickness	mm	1.90 min 15.70 max 7.30 avg. (men) 6.84 avg. (women)	r (VAT) = 0.798 r (WC) = 0.74

ROC, receiver operating curve; WC, waist circumference.

the use of contrast agents to enhance the visualization of cardiovascular anatomy and can provide improved delineation of epicardial adipose tissue. CCTA is a contrast-enhanced scan that visualizes coronary arteries, providing high-resolution images of the heart and adjacent structures. The enhanced detail allows for precise visualization of EAT. However, the use of contrast agents can pose risks to patients with allergies or other impairments. In contrast, CAC scoring is a non-contrast scan that detects coronary calcification. This imaging technique also delineates cardiac structures, contrasting epicardial fat from other tissues. La Grutta et al. (2016) compared the quantification metrics of EAT of CCTA and CAC. In their study of 76 patients suspected of CAD, the researchers measured EAT volume and thickness with semi-automatic software. The EAT volume was measured to be 122 ± 50 cm^3 for CAC scoring and 101 ± 47 cm^3 for CCTA. They noted no significant difference in median values and concluded that both imaging techniques may be equally employed for EAT assessment. Nevertheless, it is important to note that the most accurate quantification of EAT is achieved using thin-slice, non-enhanced CT images, which remain the gold standard for minimizing variability and avoiding contrast-related attenuation bias (Balcer et al., 2020; Xu et al., 2022).

4.3.2 CAT segmentation

Even though manual tracing is time-consuming, manual epicardial fat volume (EFV) segmentation procedures are currently widely used in clinical practice due to their accuracy and interpretability. Computer-aided tools have partially elevated the burden by enhancing repeatability and reducing processing time. However, this method remains costly. Semi-automated imaging techniques, such as thresholding in CT images, have further streamlined segmentation. These approaches rely on Hounsfield Unit (HU) values to identify AT, with a broad attenuation range of −250 HU to −30 HU encompassing the entire spectrum associated with fat (Marwan and Achenbach, 2013). More specifically, lower thresholds for fat detection range from −250 to −190 HU, whereas upper thresholds are generally set between −50 and −30 HU. A commonly applied reference range for fat segmentation is −130 to −30 HU (Yin et al., 2022). Importantly, differences in threshold selection can significantly affect volume estimation, particularly in contrast-enhanced CT scans. Applying the commonly reported upper limit of −30 HU for both enhanced and non-enhanced datasets has been shown to underestimate epicardial fat volumes in contrast-enhanced scans. To minimize systematic bias, semiautomated software often adjusts thresholds, with optimal upper limits reported as −43 HU for unenhanced datasets and −15 HU for contrast-enhanced scans. With the emergence of artificial intelligence (AI) in recent years, particularly deep learning (DL) methods, fully automated, fast, and highly accurate CAT segmentations are now achievable (He et al., 2020; Bencevic et al., 2021; Commandeur et al., 2019). Automatic DL methods can be generalized in a two-stage process: the first stage is to localize the heart boundary in the 3D volume, and the second stage is to delineate the pericardium (Commandeur et al., 2019). Unlike traditional methods, the DL model uses the direct training data to make CAT predictions without manual intervention. With the increase in more annotated databases and strong research interest, DL methods continue to improve. Strong results in CAT prediction accuracy have been achieved, as shown in Figure 9. However, DL efforts still rely on expert tracing as ground truth to compare the predictions. Table 3 shows automatic and semi-automatic studies to quantify CAT in CT.

TABLE 6 Comparison of main medical imaging modalities for CAT segmentation and quantification.

Feature	MRI	CT	Echocardiography
Examination time	Longer scan time	Fast acquisition time	Real-time imaging
Cost	High	Moderate	Low
Image quality	High spatial and temporal resolution, Multiplanar imaging capabilities, High soft tissue contrast, excellent for fat quantification	Good spatial resolution, accurate fat attenuation, good for calcium scoring	Lower resolution, limited depth penetration
CAT assessment	Accurate quantification, can differentiate fat types	Good for assessing fat distribution, but less accurate for quantification	Limited ability to quantify fat, primarily qualitative assessment, free wall of RV thickness
CAT quantification	Volume, thickness	Volume, thickness	Thickness
Contraindications	Contraindicated for patients with certain metal implants	Can be performed on patients with pacemakers/defibrillators	None
Constraints	Difficult for claustrophobic and robust patients, requires specialized cardiac MRI protocols	Motion artifacts can affect image quality, may require contrast agents	Difficulty in imaging obese patients, limited field of view, operator-dependent
Availability	Widely available	Widely available	Widely available
Infrastructure	Large, requires a shielded room	Moderate size room	Minimal, portable
Radiation exposure	None	High radiation dose	Minimal or no radiation
Contrast requirement	Often (gadolinium; not nephrotoxic—caution in severe renal failure)	Often (iodine-based; nephrotoxic risk)	Rare (used in contrast echo in specific cases)
Clinical feasibility	Cardiac function, tissue characterization, perfusion imaging	Chest imaging, vascular imaging	Cardiac function, valve assessment, cardiac chamber dimensions
Primary clinical applications	Tissue viability, myocarditis, cardiomyopathy, function	CAD, plaque burden, anatomy	Valve disease, EF, wall motion, pericardial effusion

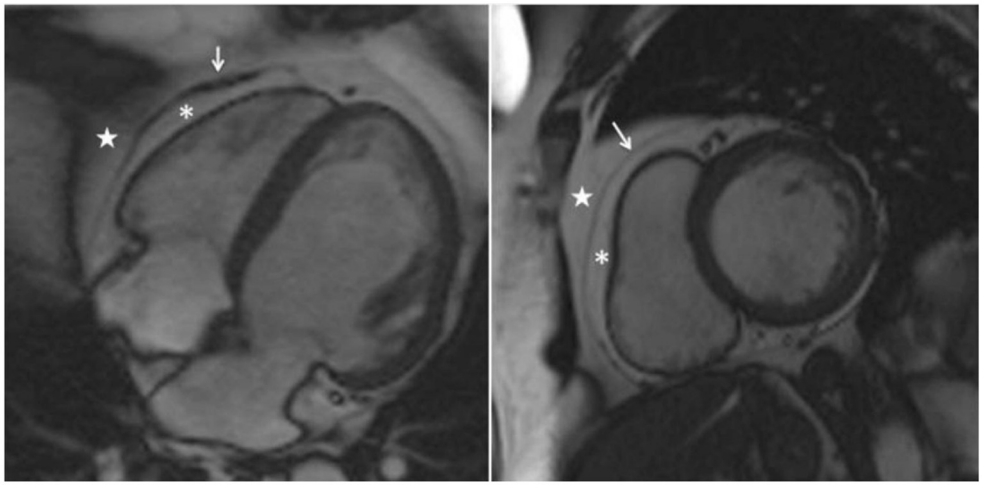

FIGURE 6
Characterization of EAT (asterisk), PAT (star), and pericardium (arrow) for MRI on long-axis four-chamber view **(left)** and basal short-axis view **(right)** at end-diastole frame (Bertaso et al., 2013).

4.3.3 CAT quantification

Once segmented, quantification of the volume and thickness of CAT is necessary to assess CVD risk. Two primary metrics, CAT volume and CAT density, are used to quantify EAT. CAT volume reflects the total fat accumulation around the heart and has been associated with the prevalence and recurrence of atrial fibrillation (AF), as well as with atherosclerosis, myocardial infarction (MI), and coronary artery calcification (CAC; Schneider et al., 2010). On the other hand, CAT density is correlated with inflammation and is linked to plaque presence and progression (Hell et al., 2016b,a). It is increasingly recognized as a biomarker of tissue composition and metabolic activity. Density reflects the relative lipid and water content within adipose tissue; higher HU values indicate reduced lipid content and increased water or fibrotic components, often

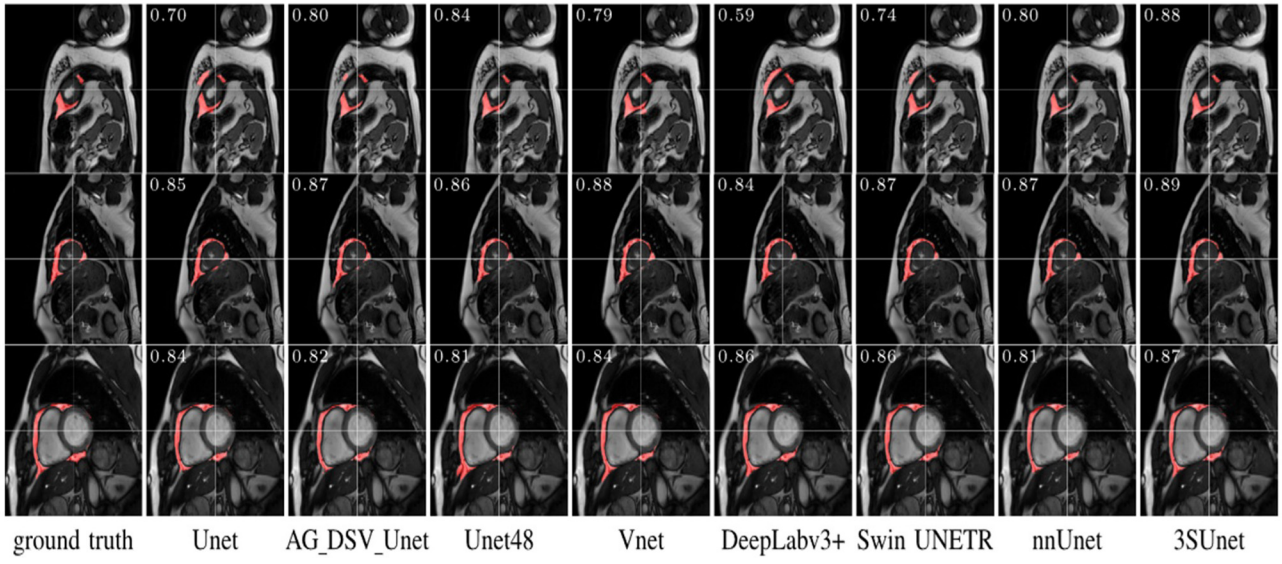

FIGURE 7
Segmentation comparison of DL models with corresponding F1 in the upper left corners (Chen et al., 2023).

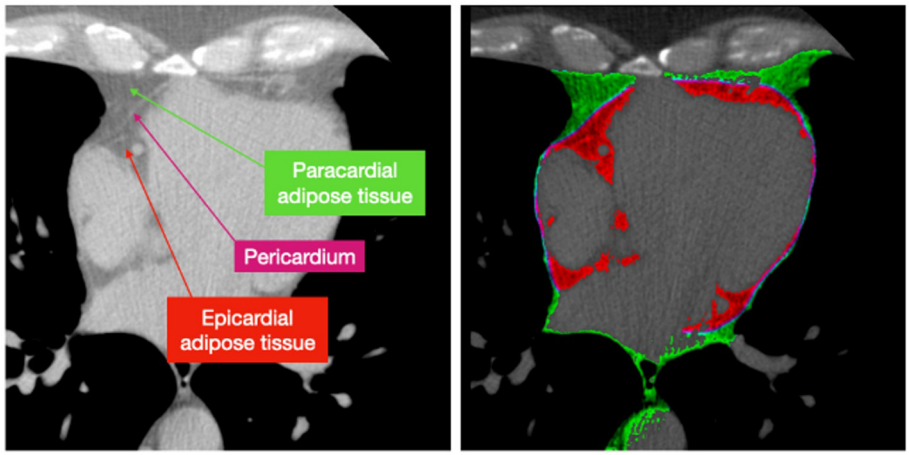

FIGURE 8
Visualization of the pericardium, EAT, and PAT on CT (Benčević et al., 2022).

associated with local inflammation. This principle parallels other imaging biomarkers, such as myosteatosis or myocardial steatosis, where fat infiltration lowers muscle density and predicts tissue degeneration and functional decline (Anumonwo and Herron, 2018). Also, elevated epicardial or pericoronary adipose tissue density has been linked to coronary inflammation and high-risk plaque features, as demonstrated by studies using the Fat Attenuation Index (FAI; Goeller et al., 2018; Klüner et al., 2021).

CAT volume can be quantified by counting the number of fat voxels (measured in Hounsfield Units) inside the pericardium border. The total volume can be estimated by summing the interslice volumes across all CT slices. The mean CAT density can be obtained by computing the mean attenuation across all slices (Commandeur et al., 2019). Automation of the quantification task significantly reduces the time burden, diminishes the variability of tracings by different observers, and results in high reproducibility. When measuring EAT volume on axial CT images, the superior-to-inferior boundary is critical for consistency. Most studies define the superior limit at the pulmonary artery bifurcation or the origin of the main pulmonary artery, and the inferior limit at the cardiac apex (Xu et al., 2022; Commandeur et al., 2019). This ensures that the entire pericardial sac is included without extending into mediastinal fat. Some protocols also use anatomical landmarks such as the left main coronary artery for the superior boundary and the diaphragmatic surface of the heart for the inferior boundary (Dey et al., 2012).

Currently, DL methods are being extended from segmentation to include quantification. Recently, Abdulkareem et al. (2022) proposed the first DL method to simultaneously quantify both EAT volume and density, building on the Commandeur et al. (2019)

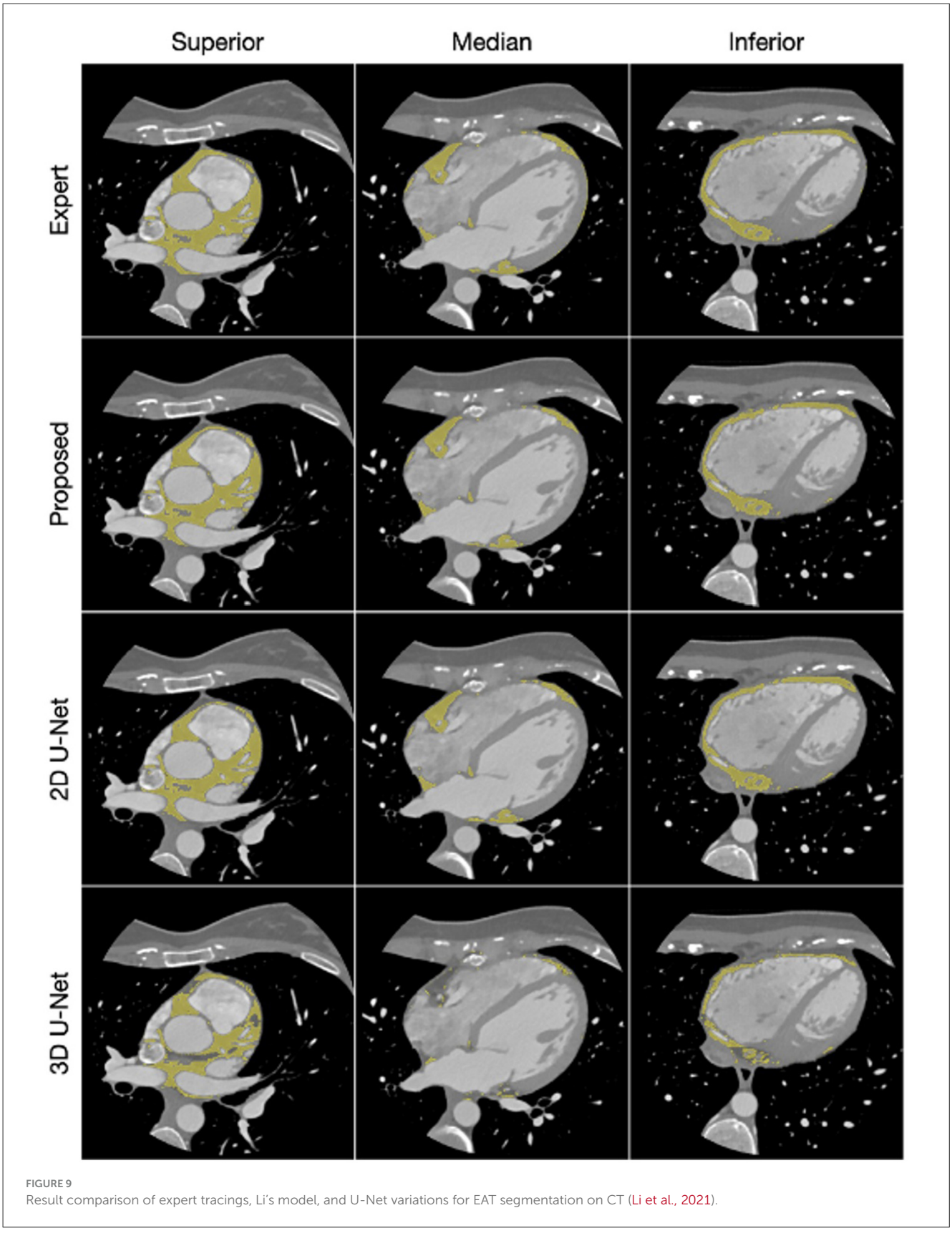

FIGURE 9
Result comparison of expert tracings, Li's model, and U-Net variations for EAT segmentation on CT (Li et al., 2021).

and Li et al. (2021) approaches to segment and quantify CAT volume. One notable investigation is the EPIDIAB Study (Gaborit et al., 2024), a multicenter trial involving 1,253 patients with type 2 diabetes. In this study, researchers developed and validated a fully automated DL model for quantifying EAT volume from cardiac CT scans. The analysis revealed strong associations between

higher EAT volumes and the presence of chronic kidney disease, coronary artery disease, peripheral arterial disease, and increased coronary artery calcium scores. These findings highlight the clinical importance of EAT as a marker of systemic vascular risk in patients with metabolic disorders. Table 4 shows the quantitative results of manual and automatic efforts to measure CAT density and volume.

4.3.4 Limitations

While CT can be more accessible than MRI, CT remains a high-cost imaging modality with limited availability. CT also exposes patients to ionizing radiation, which can pose health risks, especially in repeated imaging protocols. Moreover, artifacts are common in CT images, reducing the quality of images and complicating accurate EAT and PAT assessments. For example, partial volume effects can blur tissue types together, resulting in a single voxel containing multiple tissues. This issue can cause over- or underestimation of volume or density. Existing fully automatic methods show promising results to combat limitations and improve efficacy. However, segmentation and quantification results are still equal to or inferior to inter-observer variability (Benčević et al., 2022). A major limitation hindering progress is the lack of large, annotated datasets. The development and release of publicly available, well-labeled datasets are critical to enhance model training and improve generalizability.

From a technical perspective, coronary artery calcium (CAC) scoring scans differ from routine non-contrast chest CT in that CAC scans are ECG-gated to the cardiac cycle, reducing motion artifacts and improving visualization of cardiac structures. This gating makes CAC scans particularly suitable for accurate epicardial adipose tissue (EAT). Incorporating routine CAT segmentation into CAC scoring protocols could be a cost-effective strategy, leveraging existing imaging workflows to avoid additional radiation exposure and reduce time and resource utilization. Several studies have demonstrated feasibility of EAT quantification from CAC scans and even non-gated chest CT, though gating remains advantageous for precision (Xu et al., 2022; Commandeur et al., 2019).

4.4 Echocardiography

Echocardiography, which utilizes the principles of ultrasound (US), is a low-cost and non-invasive diagnostic and therapeutic imaging modality that offers real-time visualization of internal anatomic structures. This modality utilizes a transducer to transmit low-energy, high-frequency sound waves (typically in the 3–30 MHz range) into the body. These ultrasound signals interact with various tissue layers, and the resulting reflected echoes are captured by the transducer and processed to create diagnostic images (Vajihi et al., 2019; Insana, 2010). Echocardiograms typically employ grayscale or B-mode images as presented in Figures 10, 11. These images are constructed based on the envelope of the received ultrasound wave signals and offer detailed cross-sectional views of the heart in real time, making echocardiography an essential tool for evaluating cardiac performance and surrounding fat structures such as adipose tissue.

4.4.1 Imaging techniques

US waves are highly attenuated by bones and air, which poses significant limitations for cardiac imaging. Two principal approaches are employed: transthoracic echocardiography (TTE) and transesophageal echocardiography (TEE; Finel, 2018). When performing TTE, images are acquired through specific acoustic windows, namely: (1) parasternal, (2) apical, or (3) subcostal, and (4) suprasternal as shown in Figure 10. On each window, by tilting, rotating, and translating the transducer, different views of the cardiac structures can be obtained. Quantitative US (QUS) is a US imaging technique that involves signal processing methods used on the sound waves to provide estimates of the attenuation and backscattering properties of the interrogated tissue. Some clinical applications of QUS include the diagnosis of fatty liver disease, the detection of preterm birth risk, and the characterization of thyroid and kidney nodules (Vajihi et al., 2019).

4.4.2 CAT segmentation

The segmentation of AT using echocardiograms is a complex task that requires expertise, time investment, and good image quality. Image quality is affected by several factors such as low image contrast, shadows from body structures (ribs and dense muscles), varying speckle noise, and low signal-to-noise ratio (Chen et al., 2020). Many studies have focused on the segmentation of the main cardiac structures, targeting the measurement of the LV area and volume, subsequently used to compute EF, one of the most relevant parameters for cardiac risk assessment (Chen et al., 2020; Leclerc et al., 2019; MoosaviTayebi, 2014; Painchaud et al., 2022; Zyuzin et al., 2020; Cuellar et al., 2024). Studies using QUS have employed predefined ROIs to classify them as containing AT or not containing AT (Klingensmith et al., 2022), or have used the contours of the epicardium to segment and classify AT around the heart (Cuellar et al., 2024). A limited number of investigations identified on CAT segmentation via US were found; this underscores the critical need for further exploration in this domain, leading to a more precise, comprehensive, fast, and reliable CAT quantification.

4.4.3 CAT quantification

Transthoracic echocardiography (TTE) is used for the quantification of EAT using ultrasound (US). Parasternal long axes (PLAX) and parasternal short axes (PSAX) echocardiographic views are used for EAT quantification because they allow the most accurate measurements (Iacobellis et al., 2003). The free wall of the right ventricle has been identified as having the highest absolute adipose tissue thickness, making it ideal for consistent and reliable measurements that are less influenced by myocardial hypertrophy (Schejbal, 1989). In this area of the heart, the adipose tissue is most easily visible, and appears as an echo-free space between the visceral layer of the pericardium and the outer wall of the myocardium as shown in Figure 11 (Gaborit et al., 2017).

In the study performed by Iacobellis (Iacobellis et al., 2003), measurements of EAT thickness were correlated with anthropometric variables related to obesity. Their quantification of EAT varies between 1.9 to 15.7 mm with an average thickness of

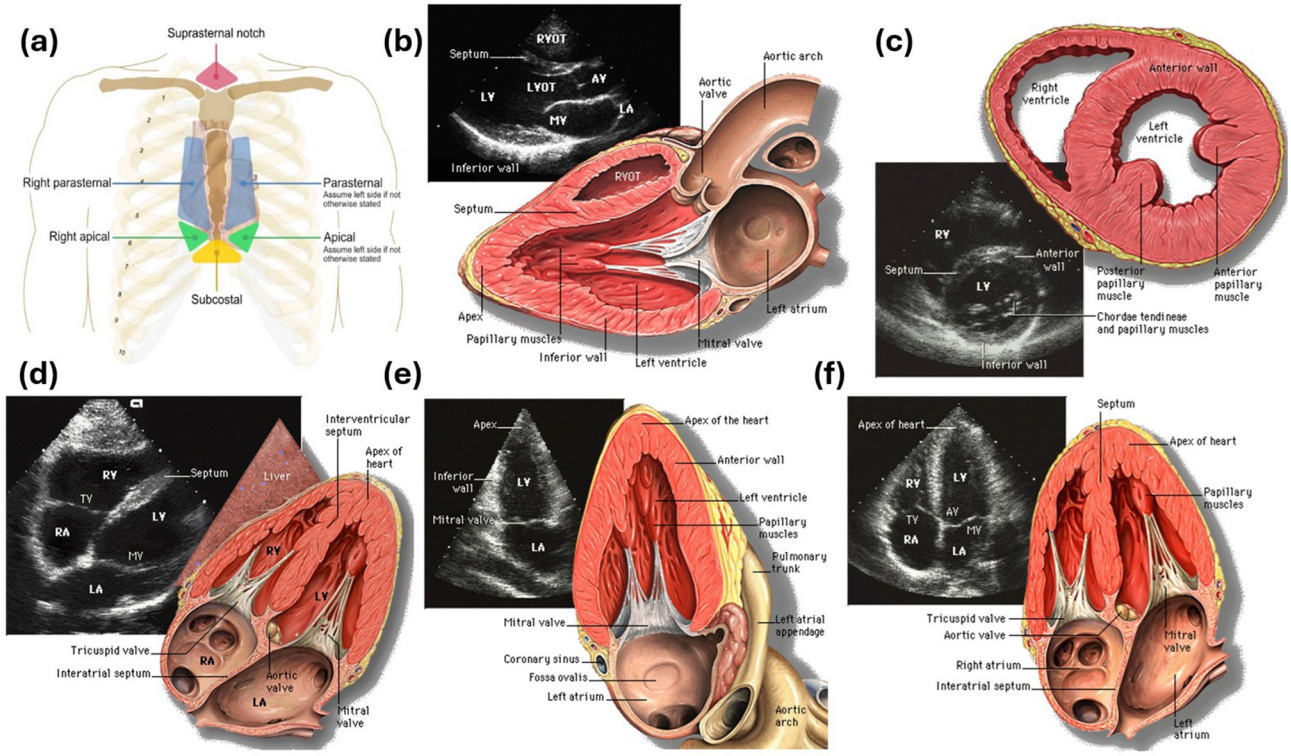

FIGURE 10
Transthoracic echocardiography (TTE). **(a)** TTE acoustic windows (Cardiovascular Education, 2019), **(b)** parasternal long axis view—PLAX; RVOT, Right ventricular outflow tract; LVOT, Left Ventricular Outflow Tract; AV, Aortic Valve; MV, Mitral Valve, LA, Left Atrium, LV, Left Ventricle, **(c)** parasternal short axis view—PSAX (top right), **(d)** subcostal view—SC; TV, Tricuspid Valve, **(e)** apical two-chamber view—A2C, and **(f)** apical four-chamber view—A4C (Patrick Lynch, 2017).

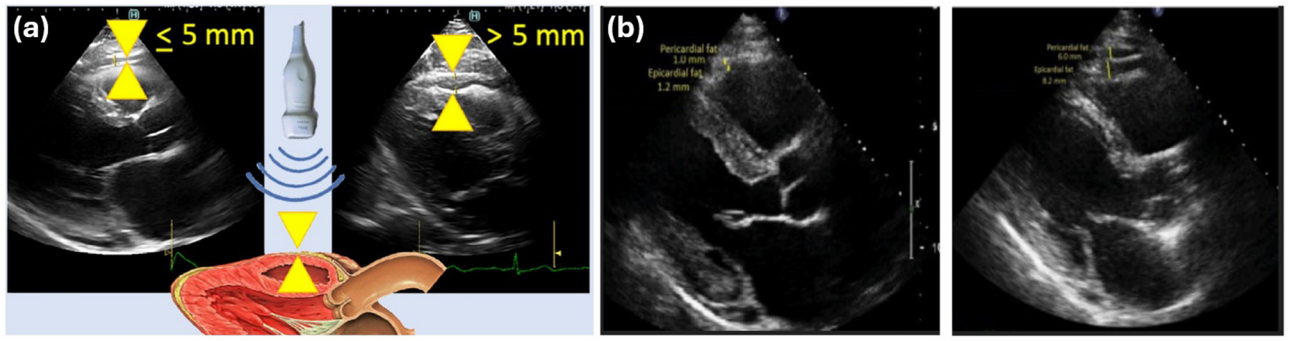

FIGURE 11
Fat quantification in ultrasound, **(a)** EAT linear measurements perpendicular to the aortic annulus below and above a 5 mm threshold (Nesti et al., 2023), **(b)** differentiation between EAT and PAT in echocardiograms (Sicari et al., 2011).

7.3 ± 3.42 mm in men, and 6.84 ± 2.76 mm in women. To avoid oblique measurements of EAT using US, in Nesti et al. (2023), measurements have been taken perpendicular to the aortic annulus, using it as an anatomic landmark, as shown in Figure 11a. Some studies have shown their ability to differentiate and measure EAT and PAT thicknesses as illustrated in Figure 11b (Sicari et al., 2011). Table 5 summarizes the studies found in this literature review where the CAT thickness measured over the RV was identified as a marker for several types of CAD.

4.4.4 Limitations

Compared with MRI and CT, the main limitation of echocardiography is image resolution. In addition, fat quantification is limited to linear thickness measurements in particular locations without volumetric computations (Nerlekar et al., 2018), and the differentiation between EAT and PAT is not possible (Iacobellis et al., 2008). Finally, the accuracy and reproducibility of the adipose thickness measurements have lower precision when compared to other imaging modalities (Song

et al., 2023). US imaging is limited by anatomical constraints, making it impossible to image the heart from all angles and positions. Certain crucial regions, such as those adjacent to the coronary arteries, where fat depositions are highly correlated with plaque development, are often challenging to image using echocardiography.

5 Discussion

In conclusion, this review has explored various medical imaging modalities to assess the multifaceted relationship between adipose tissue and cardiovascular health. We examined the distinct types of fat surrounding the heart, highlighting the potential role of CAT in promoting cardiovascular disease. MRI, CT, and echocardiography were identified as the primary imaging modalities for assessing cardiac fat, each offering unique advantages and limitations in segmentation and quantification. Recent advancements in cardiovascular imaging have significantly deepened our understanding of the relationship between EAT and cardiovascular disease risk. Several prospective and retrospective studies have demonstrated the clinical value of quantifying EAT and PAT using automated imaging and deep learning tools. Guglielmo et al. (2024) studied 730 patients who underwent stress CMR. His study showed that increased EAT volume, as quantified from CMR images, was an independent predictor of major adverse cardiovascular events—including non-fatal myocardial infarctions and cardiac deaths. Li et al. (2022) developed and tested PAT-CNN in a study conducted on 391 patients. He found that higher PAT volumes were not only associated with existing cardiovascular disease diagnoses but also served as independent predictors of 1-year all-cause mortality. Commandeur et al. explored "fat-omics," a novel approach using handcrafted radiomic features derived from EAT. The incorporation of these features into predictive models significantly improved the prediction of major adverse cardiovascular events (MACE), reinforcing the biological and clinical relevance of EAT beyond its volume. This evidence supports the notion that EAT is not merely a passive fat depot but may actively contribute to inflammation, atherosclerosis, and myocardial dysfunction (Hu et al., 2024). Eisenberg et al. (2020) introduced a deep-learning model capable of accurately quantifying EAT volume using cardiac CT angiography. This automated approach not only demonstrated high reproducibility but also proved effective in technically challenging patients, highlighting the clinical utility of artificial intelligence in enhancing EAT assessment. The accompanying editorial emphasized that such automation could standardize EAT measurement across institutions and help integrate this metric into routine cardiovascular risk assessment workflows. Grinspoon et al. evaluated the use of tesamorelin on visceral fat reduction in HIV-infected patients revealed insights into the metabolic behavior of fat depots adjacent to the heart (Stanley et al., 2014). While EAT was not the primary focus, the implications for how regional fat impacts systemic inflammation and cardiovascular health remain highly relevant. Together, these studies suggest a paradigm shift where adipose tissue—traditionally considered secondary—may serve as a central player in cardiovascular diagnostics. The results of these studies reinforce the prognostic value of EAT in routine cardiac imaging and suggest its utility in risk stratification. The use of deep learning for PAT analysis presents an opportunity to explore less commonly evaluated fat depots with significant clinical implications. Also, these studies emphasize the growing importance of integrating machine learning with advanced imaging to enhance the precision of cardiac fat quantification. Such approaches hold promise for improving early disease detection, refining cardiovascular risk models, and personalizing therapeutic interventions based on adipose tissue burden. In addition, the findings highlight the important need for consistent and standardized imaging methods, along with reliable tools to measure epicardial adipose tissue (EAT) accurately. Without such standards, it becomes difficult to compare results across studies or apply them in clinical settings. As research continues to uncover the specific roles of both EAT and pericardial adipose tissue (PAT) in heart disease, combining advanced imaging technologies with machine learning offers a promising path. This approach could not only improve early diagnosis of cardiovascular conditions but also help tailor treatment strategies to each patient's individual risk profile, ultimately improving outcomes.

Table 6 summarizes and compares the key features offered for each imaging modality for CAT segmentation and quantification. While significant advancements have been made, challenges remain in accurately measuring and interpreting fat distribution around the heart. Future research efforts should focus on refining segmentation techniques, establishing standardized protocols, and elucidating the specific mechanisms by which adipose tissue contributes to cardiovascular risk. By addressing these limitations, we can leverage the power of cardiac fat imaging to improve risk stratification, guide treatment strategies, and promote better cardiovascular health outcomes.

Author contributions

JC: Investigation, Resources, Visualization, Writing – original draft, Funding acquisition. MBh: Writing – review & editing. MBu: Writing – review & editing. PC: Investigation, Visualization, Writing – original draft. JK: Funding acquisition, Writing – review & editing.

Funding

The author(s) declared that financial support was received for this work and/or its publication. This work was supported by the American Heart Association -AHA (Predoctoral fellowship; https://doi.org/10.58275/AHA.24PRE1188140.pc.gr.190654 to Julian Rene Cuellar Buritica).

Conflict of interest

The author(s) declared that this work was conducted in the absence of any commercial or financial relationships that could be construed as a potential conflict of interest.

Generative AI statement

The author(s) declared that generative AI was not used in the creation of this manuscript.

Any alternative text (alt text) provided alongside figures in this article has been generated by Frontiers with the support of artificial intelligence and reasonable efforts have been made to ensure accuracy, including review by the authors wherever possible. If you identify any issues, please contact us.

Publisher's note

References

Abdulkareem, M., Brahier, M. S., Zou, F., Rauseo, E., Uchegbu, I., Taylor, A., et al. (2022). Quantification of epicardial adipose tissue volume and attenuation for cardiac CT scans using deep learning in a single multi-task framework. *Rev. Cardiovasc. Med.* 23:412. doi: 10.31083/j.rcm2312412

Ahmed, N., Carrick, D., Layland, J., Oldroyd, K. G., and Berry, C. (2013). The role of cardiac magnetic resonance imaging (MRI) in acute myocardial infarction (AMI). *Heart Lung Circul.* 22, 243–255. doi: 10.1016/j.hlc.2012.11.016

Alkhalil, M., Edmond, E., Edgar, L., Digby, J. E., Omar, O., Robson, M. D., et al. (2018). The relationship of perivascular adipose tissue and atherosclerosis in the aorta and carotid arteries, determined by magnetic resonance imaging. *Diabetes Vasc. Dis. Res.* 15, 286–293. doi: 10.1177/1479164118757923

Antonopoulos, A. S., and Antoniades, C. (2018). Cardiac magnetic resonance imaging of epicardial and intramyocardial adiposity as an early sign of myocardial disease. *Circulation Cardiovasc. Imag.* 11:e008083. doi: 10.1161/CIRCIMAGING.118.008083

Anumonwo, J. M. B., and Herron, T. (2018). Fatty infiltration of the myocardium and arrhythmogenesis: potential cellular and molecular mechanisms. *Front. Physiol.* 9:2. doi: 10.3389/fphys.2018.00002

Bachar, G. N., Dicker, D., Kornowski, R., and Atar, E. (2012). Epicardial adipose tissue as a predictor of coronary artery disease in asymptomatic subjects. *Am. J. Cardiol.* 110, 534–538. doi: 10.1016/j.amjcard.2012.04.024

Balcer, B., Rassaf, T., and Mahabadi, A. A. (2020). "Computed tomography imaging of epicardial adipose tissue," in *Epicardial Adipose Tissue*, ed. G. Iacobellis (Cham: Springer International Publishing), 55–70. Available online at: http://link.springer.com/10.1007/978-3-030-40570-0_6 doi: 10.1007/978-3-030-40570-0_6 (Accessed November 3, 2025).

Benčević, M., Galić, I., Habijan, M., and PiŽurica, A. (2022). Recent progress in epicardial and pericardial adipose tissue segmentation and quantification based on deep learning: a systematic review. *Appl. Sci.* 12:5217. doi: 10.3390/app12105217

Bencevic, M., Habijan, M., and Galic, I. (2021). "Epicardial adipose tissue segmentation from CT images with A semi-3D neural network," in *2021 International Symposium ELMAR* (Zadar: IEEE), 87–90. Available online at: https://ieeexplore.ieee.org/document/9550936/ (Accessed July 1, 2024).

Bertaso, A. G., Bertol, D., Duncan, B. B., and Foppa, M. (2013). Epicardial fat: definition, measurements and systematic review of main outcomes. *Arquivos Brasileiros Cardiol.* 101. doi: 10.5935/abc.20130138

Cardiovascular Education (2019). *Standard Transthoracic Echocardiogram: Complete Imaging Protocol.* Available online at: https://ecgwaves.com/topic/the-standard-adult-transthoracic-echocardiogram-a-protocol-to-obtain-a-complete-study/ (Accessed July 8, 2024).

Cheładze, P., Martuszewski, A., Poreba, R., and Gać, P. (2022). The importance of the assessment of epicardial adipose tissue in scientific research. *J. Clin. Med.* 11:5621. doi: 10.3390/jcm11195621

Chen, C., Qin, C., Qiu, H., Tarroni, G., Duan, J., Bai, W., et al. (2020). Deep learning for cardiac image segmentation: a review. *Front. Cardiovasc. Med.* 7:25. doi: 10.3389/fcvm.2020.00025

Chen, S., An, D., Feng, C., Bian, Z., and Wu, L. M. (2023). Segmentation of pericardial adipose tissue in CMR images: a benchmark dataset MRPEAT and a triple-stage network 3SUnet. *IEEE Trans. Med. Imag.* 42, 2386–2399. doi: 10.1109/TMI.2023.3251368

Chhabra, L., and Gurukripa Kowlgi, N. (2015). Cardiac adipose tissue: distinction between epicardial and pericardial fat remains important! *Int. J. Cardiol.* 201, 274–275. doi: 10.1016/j.ijcard.2015.08.068

Cleveland Clinic, Z. Z. (2023). *What's Draggin' Your Heart Down?* Available online at: https://my.clevelandclinic.org/health/diseases/16898-coronary-artery-disease (Accessed May 29, 2024).

Commandeur, F., Goeller, M., Betancur, J., Cadet, S., Doris, M., Chen, X., et al. (2018). Deep learning for quantification of epicardial and thoracic adipose tissue from non-contrast CT. *IEEE Trans. Med. Imag.* 37, 1835–1846. doi: 10.1109/TMI.2018.2804799

Commandeur, F., Goeller, M., Razipour, A., Cadet, S., Hell, M. M., Kwiecinski, J., et al. (2019). Fully automated CT quantification of epicardial adipose tissue by deep learning: a multicenter study. *Radiol. Artificial Intell.* 1:e190045. doi: 10.1148/ryai.2019190045

Cuellar, J. R., Dinh, V., Burri, M., Roelandts, J., Wendling, J., Klingensmith, J. D., et al. (2025). Evaluation of state-of-the-art deep learning models in the segmentation of the left and right ventricles in parasternal short-axis echocardiograms. *J. Med. Imag.* 12:024002. doi: 10.1117/1.JMI.12.2.024002

Cuellar, J. R., Gillette, L., Dinh, V., Woodard, P., Burri, M., Klingensmith, J. D., et al. (2024). "Echocardiogram image segmentation and cardiac adipose tissue estimation using spectral analysis and deep learning," in *Proceedings of SPIE 12932, Medical Imaging 2024: Ultrasonic Imaging and Tomography*, 129320C. doi: 10.1117/12.3004836

Curtis, A. D., and Cheng, H. M. (2022). Primer and historical review on rapid cardiac CINE MRI. *Magnetic Resonance Imag.* 55, 373–388. doi: 10.1002/jmri.27436

Daudé, P., Ancel, P., Confort Gouny, S., Jacquier, A., Kober, F., Dutour, A., et al. (2022). Deep-learning segmentation of epicardial adipose tissue using four-chamber cardiac magnetic resonance imaging. *Diagnostics* 12:126. doi: 10.3390/diagnostics12010126

Demmert, T. T., Klambauer, K., Moser, L. J., Mergen, V., Eberhard, M., Alkadhi, H., et al. (2025). Epicardial and pericardial adipose tissue: anatomy, physiology, imaging, segmentation, and treatment effects. *Br. J. Radiol.* 2025:tqaf223. doi: 10.1093/bjr/tqaf223

D'Errico, L., Salituri, F., Ciardetti, M., Favilla, R., Mazzarisi, A., Coppini, G., et al. (2017). Quantitative analysis of epicardial fat volume: effects of scanning protocol and reproducibility of measurements in non-contrast cardiac CT vs. coronary CT angiography. *Quant Imag. Med Surg.* 7, 326–335. doi: 10.21037/qims.2017.06.08

Dey, D., Nakazato, R., Slomka, P. J., and Berman, D. S. (2012). CT quantification of epicardial fat: implications for cardiovascular risk assessment. *Curr. Cardiovasc. Imag. Rep.* 5, 352–359. doi: 10.1007/s12410-012-9154-4

Ding, J., Hsu, F. C., Harris, T. B., Liu, Y., Kritchevsky, S. B., Szklo, M., et al. (2009). The association of pericardial fat with incident coronary heart disease: the Multi-Ethnic Study of Atherosclerosis (MESA). *Am. J. Clin. Nutr.* 90, 499–504. doi: 10.3945/ajcn.2008.27358

Ding, J., Kritchevsky, S. B., Harris, T. B., Burke, G. L., Detrano, R. C., Szklo, M., et al. (2008). The association of pericardial fat with calcified coronary plaque. *Obesity* 16, 1914–1919. doi: 10.1038/oby.2008.278

Drake, R., Vogl, A. W., and Mitchell, A. W. M. (2014). *Gray's Anatomy for Students E-Book*. Elsevier Health Sciences, 1191p. Available online at: https://books.google.com/books?id=Lh20BQAAQBAJ&lpg=PP1&pg=PP1#v=onepage&q&f=false

Eisenberg, E., McElhinney, P. A., Commandeur, F., Chen, X., Cadet, S., Goeller, M., et al. (2020). Deep Learning–based quantification of epicardial adipose tissue volume and attenuation predicts major adverse cardiovascular events in asymptomatic subjects. *Circ. Cardiovasc. Imag.* 13:e009829. doi: 10.1161/CIRCIMAGING.119.009829

Eren, H., Omar, M. B., and Öcal, L. (2021). Epicardial fat tissue may predict new-onset atrial fibrillation in patients with non-ST-segment elevation myocardial infarction. *Arch. Turkish Soc. Cardiol.* 49, 430–438. doi: 10.5543/tkda.2021.50759

Farese, R. V., and Walther, T. C. (2009). Lipid droplets finally get a little R-E-S-P-E-C-T. *Cell* 139, 855–860. doi: 10.1016/j.cell.2009.11.005

Feng, F., Carlhäll, C. J., Tan, Y., Agrawal, S., Lundberg, P., Bai, J., et al. (2024). "FM-Net: a fully automatic deep learning pipeline for epicardial adipose tissue segmentation," in *Statistical Atlases and Computational Models of the Heart Regular and CMRxRecon Challenge Papers*, eds. O. Camara, E. Puyol-Antón, M. Sermesant, A.

Suinesiaputra, Q. Tao, C. Wang, et al. (Cham: Springer Nature Switzerland), 88–97. (Lecture Notes in Computer Science; vol. 14507). Available online at: https://link.springer.com/10.1007/978-3-031-52448-6_9 (Accessed May 28, 2024).

Finel, V. (2018). *3D ultrafast echocardiography* (Doctoral thesis). Sorbonne, Paris, France.

Fitzgibbons, T. P., and Czech, M. P. (2014). Epicardial and perivascular adipose tissues and their influence on cardiovascular disease: basic mechanisms and clinical associations. *JAHA* 3:e000582. doi: 10.1161/JAHA.113.000582

Flohr, T., Schmidt, B., Ulzheimer, S., and Alkadhi, H. (2023). Cardiac imaging with photon counting CT. *Br. J. Radiol*. 96:20230407. doi: 10.1259/bjr.20230407

Fulton, M. R., Givan, A. H., Fernandez-del-Valle, M., and Klingensmith, J. D. (2020). "Segmentation of epicardial adipose tissue in cardiac MRI using deep learning," in *Proc. SPIE 11317, Medical Imaging 2020: Biomedical Applications in Molecular, Structural, and Functional Imaging,* 113170Q. doi: 10.1117/12.2550013

Gaborit, B., Julla, J. B., Fournel, J., Ancel, P., Soghomonian, A., Deprade, C., et al. (2024). Fully automated epicardial adipose tissue volume quantification with deep learning and relationship with CAC score and micro/macrovascular complications in people living with type 2 diabetes: the multicenter EPIDIAB study. *Cardiovasc. Diabetol*. 23:328. doi: 10.1186/s12933-024-02411-y

Gaborit, B., Sengenes, C., Ancel, P., Jacquier, A., and Dutour, A. (2017). Role of epicardial adipose tissue in health and disease: a matter of fat? *Comprehens. Physiol*. 7, 1051–1082. doi: 10.1002/cphy.c160034

Gaeta, M., Bandera, F., Tassinari, F., Capasso, L., Cargnelutti, M., Pelissero, G., et al. (2017). Is epicardial fat depot associated with atrial fibrillation? A systematic review and meta-analysis. *Europace* 19, 747–752. doi: 10.1093/europace/euw398

Gaillard, F. (2025). *Radiopaedia. Lipomatous Hypertrophy of the Interatrial Septum*. Radiology Reference Article | Radiopaedia.org. Available online at: https://radiopaedia.org/articles/lipomatous-hypertrophy-of-the-interatrial-septum?lang=us (Accessed May 29, 2024).

Ginzburg, D., Nowak, S., Attenberger, U., Luetkens, J., Sprinkart, A. M., Kuetting, D., et al. (2024). Computer tomography-based assessment of perivascular adipose tissue in patients with abdominal aortic aneurysms. *Sci. Rep*. 14:20512. doi: 10.1038/s41598-024-71283-9

Goeller, M., Achenbach, S., Cadet, S., Kwan, A. C., Commandeur, F., Slomka, P. J., et al. (2018). Pericoronary adipose tissue computed tomography attenuation and high-risk plaque characteristics in acute coronary syndrome compared with stable coronary artery disease. *JAMA Cardiol*. 3:858. doi: 10.1001/jamacardio.2018.1997

Greco, F., Salgado, R., Van Hecke, W., Del Buono, R., Parizel, P. M., Mallio, C. A., et al. (2022). Epicardial and pericardial fat analysis on CT images and artificial intelligence: a literature review. *Quant. Imag. Med. Surg*. 12, 2075–2089. doi: 10.21037/qims-21-945

Grigoras, A., Amalinei, C., Balan, R. A., Giusca, S. E., and Caruntu, I. D. (2019). Perivascular adipose tissue in cardiovascular diseases-an update. *Anatol. J. Cardiol*. 22, 219–231. doi: 10.14744/AnatolJCardiol.2019.91380

Guglielmo, M., Lin, A., Dey, D., Baggiano, A., Fusini, L., Muscogiuri, G., et al. (2021). Epicardial fat and coronary artery disease: role of cardiac imaging. *Atherosclerosis* 321, 30–38. doi: 10.1016/j.atherosclerosis.2021.02.008

Guglielmo, M., Penso, M., Carerj, M. L., Giacari, C. M., Volpe, A., Fusini, L., et al. (2024). DEep LearnIng-based QuaNtification of epicardial adipose tissue predicts MACE in patients undergoing stress CMR. *Atherosclerosis* 397:117549. doi: 10.1016/j.atherosclerosis.2024.117549

Gul, Z., Shams, P., and Makaryus, A. N. (2024). *Silent Myocardial Ischemia*. Treasure Island, FL: StatPearls Publishing. Available online at: http://www.ncbi.nlm.nih.gov/books/NBK536915/ (Accessed June 18, 2024).

He, X., Guo, B., Lei, Y., Wang, T., Liu, T., Curran, W. J., et al. (2020). "Automatic epicardial fat segmentation in cardiac CT imaging using 3D deep attention U-Net," in *Medical Imaging 2020: Image Processing*, eds. B. A. Landman and I. Išgum (Houston, TX: SPIE), 84. Available online at: https://www.spiedigitallibrary.org/conference-proceedings-of-spie/11313/2550383/Automatic-epicardial-fat-segmentation-in-cardiac-CT-imaging-using-3D/10.1117/12.2550383.full (Accessed May 17, 2024).

Hell, M. M., Achenbach, S., Schuhbaeck, A., Klinghammer, L., May, M. S., Marwan, M., et al. (2016a). CT-based analysis of pericoronary adipose tissue density: relation to cardiovascular risk factors and epicardial adipose tissue volume. *J. Cardiovasc. Comput. Tomogr*. 10, 52–60. doi: 10.1016/j.jcct.2015.07.011

Hell, M. M., Ding, X., Rubeaux, M., Slomka, P., Gransar, H., Terzopoulos, D., et al. (2016b). Epicardial adipose tissue volume but not density is an independent predictor for myocardial ischemia. *J. Cardiovasc. Comput. Tomogr*. 10, 141–149. doi: 10.1016/j.jcct.2016.01.009

Henningsson, M., Brundin, M., Scheffel, T., Edin, C., Viola, F., Carlhäll, C. J., et al. (2020). Quantification of epicardial fat using 3D cine Dixon MRI. *BMC Med. Imag*. 20:80. doi: 10.1186/s12880-020-00478-z

Hernandez, A., Singh, A., and Miklush, L. (2025). *Osmosis - Adipose Tissue. Adipose Tissue: What Is It, Location, Function, and More*. Available online at: https://www.osmosis.org/answers/adipose-tissue (Accessed June 6, 2024).

Hirata, Y., Yamada, H., Kusunose, K., Iwase, T., Nishio, S., Hayashi, S., et al. (2015). Clinical utility of measuring epicardial adipose tissue thickness with echocardiography using a high-frequency linear probe in patients with coronary artery disease. *J. Am. Soc. Echocardiogr*. 28, 1240–1246.e1. doi: 10.1016/j.echo.2015.07.006

Homsi, R., Meier-Schroers, M., Gieseke, J., Dabir, D., Luetkens, J. A., Kuetting, D. L., et al. (2016). 3D-Dixon MRI based volumetry of peri- and epicardial fat. *Int. J. Cardiovasc. Imag*. 32, 291–299. doi: 10.1007/s10554-015-0778-8

Hoori, A., Hu, T., Lee, J., Al-Kindi, S., Rajagopalan, S., Wilson, D. L., et al. (2022). Deep learning segmentation and quantification method for assessing epicardial adipose tissue in CT calcium score scans. *Sci. Rep*. 12:2276. doi: 10.1038/s41598-022-06351-z

Hu, T., Freeze, J., Singh, P., Kim, J., Song, Y., Wu, H., et al. (2024). Artificial intelligence prediction of cardiovascular events using opportunistic epicardial adipose tissue assessments from computed tomography calcium score. *JACC Adv*. 3:101188. doi: 10.1016/j.jacadv.2024.101188

Iacobellis, G. (2009). Epicardial and pericardial fat: close, but very different. *Obesity* 17, 625. doi: 10.1038/oby.2008.575

Iacobellis, G. (2015). Local and systemic effects of the multifaceted epicardial adipose tissue depot. *Nat. Rev. Endocrinol*. 11, 363–371. doi: 10.1038/nrendo.2015.58

Iacobellis, G. (2022). Epicardial adipose tissue in contemporary cardiology. *Nat. Rev. Cardiol*. 19, 593–606. doi: 10.1038/s41569-022-00679-9

Iacobellis, G., Assael, F., Ribaudo, M. C., Zappaterreno, A., Alessi, G., Di Mario, U., et al. (2003). Epicardial fat from echocardiography: a new method for visceral adipose tissue prediction. *Obes. Res*. 11, 304–310. doi: 10.1038/oby.2003.45

Iacobellis, G., and Willens, H. J. (2009). Echocardiographic epicardial fat: a review of research and clinical applications. *J. Am. Soc. Echocardiogr*. 22, 1311–1319. doi: 10.1016/j.echo.2009.10.013

Iacobellis, G., Willens, H. J., Barbaro, G., and Sharma, A. M. (2008). Threshold values of high-risk echocardiographic epicardial fat thickness. *Obesity* 16, 887–892. doi: 10.1038/oby.2008.6

Insana, M. (2010). *Handbook of Physics in Medicine and Biology - Ultrasonic Imaging, 0 Edn*. (ed. R. Splinter). CRC Press. Available online at: https://www.taylorfrancis.com/books/9781420075250 (Accessed July 7, 2024).

Ismail, I., Al-Khafaji, K., Mutyala, M., Aggarwal, S., Cotter, W., Hakim, H., et al. (2015). Cardiac lipoma. *J. Commun. Hosp. Intern. Med. Perspect*. 5. doi: 10.3402/jchimp.v5.28449

Karlapalem, A., Cuellar, J., Umbaugh, S. E., Marino, D. J., Sackman, J. (2019). "Detection of syrinx in thermographic images of canines with Chiari malformation using MATLAB CVIP toolbox GUI," in *Proc. SPIE 11004, Thermosense: Thermal Infrared Applications XLI*, 1100405. doi: 10.1117/12.2519112

Kim, I. K., Song, B. W., Lim, S., Kim, S. W., and Lee, S. (2023). The role of epicardial adipose tissue-derived microRNAs in the regulation of cardiovascular disease: a narrative review. *Biology* 12:498. doi: 10.3390/biology12040498

Klingensmith, J. D., Karlapalem, A., Kulasekara, M. M., and Fernandez-del-Valle, M. (2022). Spectral analysis of ultrasound radiofrequency backscatter for the identification of epicardial adipose tissue. *J. Med. Imag*. 9:017001. doi: 10.1117/1.JMI.9.1.017001

Klüner, L. V., Oikonomou, E. K., and Antoniades, C. (2021). Assessing cardiovascular risk by using the fat attenuation index in coronary CT angiography. *Radiol. Cardiothoracic Imag*. 3:e200563. doi: 10.1148/ryct.2021200563

Konwerski, M., Gasecka, A., Opolski, G., Grabowski, M., and Mazurek, T. (2022). Role of epicardial adipose tissue in cardiovascular diseases: a review. *Biology* 11:355. doi: 10.3390/biology11030355

Krauz, K., Kempiński, M., Jańczak, P., Momot, K., Zarebiński, M., Poprawa, I., et al. (2024). The role of epicardial adipose tissue in acute coronary syndromes, post-infarct remodeling and cardiac regeneration. *Int. J. Mol. Sci*. 25:3583. doi: 10.3390/ijms25073583

Kulasekara, M., Dinh, V. Q., Fernandez-del-Valle, M., and Klingensmith, J. D. (2022). Comparison of two-dimensional and three-dimensional U-Net architectures for segmentation of adipose tissue in cardiac magnetic resonance images. *Med. Biol. Eng. Comput*. 60, 2291–2306. doi: 10.1007/s11517-022-02612-1

La Grutta, L., Toia, P., Farruggia, A., Albano, D., Grassedonio, E., Palmeri, A., et al. (2016). Quantification of epicardial adipose tissue in coronary calcium score and CT coronary angiography image data sets: comparison of attenuation values, thickness and volumes. *BJR* 89:20150773. doi: 10.1259/bjr.20150773

Large, S. R., Hosseinpour, A. R., Wisbey, C., and Wells, F. C. (1997). Spontaneous cardioversion and mitral valve repair: a role for surgical cardioversion (Cox-maze)? *Eur. J. Cardiothorac. Surg*. 11, 76–80. doi: 10.1016/S1010-7940(96)01012-3

Leclerc, S., Smistad, E., Pedrosa, J., Ostvik, A., Cervenansky, F., Espinosa, F., et al. (2019). Deep learning for segmentation using an open large-scale dataset in 2D echocardiography. *IEEE Trans. Med. Imag*. 38, 2198–2210. doi: 10.1109/TMI.2019.2900516

Li, C., Liu, X., Adhikari, B. K., Chen, L., Liu, W., Wang, Y., et al. (2023). The role of epicardial adipose tissue dysfunction in cardiovascular diseases: an overview of pathophysiology, evaluation, and management. *Front. Endocrinol*. 14:1167952. doi: 10.3389/fendo.2023.1167952

Li, X., Sun, Y., Xu, L., Greenwald, S. E., Zhang, L., Zhang, R., et al. (2021). Automatic quantification of epicardial adipose tissue volume. *Med. Phys*. 48, 4279–4290. doi: 10.1002/mp.15012

Li, Z., Petri, C., Howard, J., Cole, G., and Varela, M. (2022). PAT-CNN: automatic segmentation and quantification of pericardial adipose tissue from T2-weighted cardiac magnetic resonance images. *arXiv*. Available online at: http://arxiv.org/abs/2211.04995 (Accessed June 13, 2025).

Liu, C. Y., Redheuil, A., Ouwerkerk, R., Lima, J. A. C., and Bluemke, D. A. (2010). Myocardial fat quantification in humans: evaluation by two-point water-fat imaging and localized proton spectroscopy. *Magn. Reson. Med*. 63, 892–901. doi: 10.1002/mrm.22289

Mahabadi, A. A., Kahlert, H. A., Dykun, I., Balcer, B., Kahlert, P., Rassaf, T., et al. (2017). Epicardial adipose tissue thickness independently predicts severe aortic valve stenosis. *J. Heart Valve Dis*. 26, 262–267.

Mahabadi, A. A., Massaro, J. M., Rosito, G. A., Levy, D., Murabito, J. M., Wolf, P. A., et al. (2009). Association of pericardial fat, intrathoracic fat, and visceral abdominal fat with cardiovascular disease burden: the Framingham Heart Study. *Eur. Heart J*. 30, 850–856. doi: 10.1093/eurheartj/ehn573

Mahmoud, I., Dykun, I., Kärner, L., Hendricks, S., Totzeck, M., Al-Rashid, F., et al. (2021). Epicardial adipose tissue differentiates in patients with and without coronary microvascular dysfunction. *Int. J. Obes*. 45, 2058–2063. doi: 10.1038/s41366-021-00875-6

Malavazos, A. E., Di Leo, G., Secchi, F., Lupo, E. N., Dogliotti, G., Coman, C., et al. (2010). Relation of echocardiographic epicardial fat thickness and myocardial fat. *Am. J. Cardiol*. 105, 1831–1835. doi: 10.1016/j.amjcard.2010.01.368

Malik, A., Brito, D., Vaqar, S., and Chhabra, L. (2024). *Congestive Heart Failure*. Treasure Island, FL: StatPearls Publishing. Available online at: http://www.ncbi.nlm.nih.gov/books/NBK430873/ (Accessed June 19, 2024).

Mancio, J., Azevedo, D., Saraiva, F., Azevedo, A. I., Pires-Morais, G., Leite-Moreira, A., et al. (2018). Epicardial adipose tissue volume assessed by computed tomography and coronary artery disease: a systematic review and meta-analysis. *Euro. Heart J. Cardiovasc. Imag*. 19, 490–497. doi: 10.1093/ehjci/jex314

Marwan, M., and Achenbach, S. (2013). Quantification of epicardial fat by computed tomography: why, when and how? *J. Cardiovasc. Comput. Tomogr*. 7, 3–10. doi: 10.1016/j.jcct.2013.01.002

Marwan, M., Koenig, S., Schreiber, K., Ammon, F., Goeller, M., Bittner, D., et al. (2019). Quantification of epicardial adipose tissue by cardiac CT: influence of acquisition parameters and contrast enhancement. *Euro. J. Radiol*. 121:108732. doi: 10.1016/j.ejrad.2019.108732

Mayo Clinic, Z. Z. (2024a). *Coronary Artery Disease - Symptoms and Causes*. Available online at: https://www.mayoclinic.org/diseases-conditions/coronary-artery-disease/symptoms-causes/syc-20350613 (Accessed May 29, 2024).

Mayo Clinic, Z. Z. (2024b). *Mitral Valve Stenosis - Symptoms and Causes*. Available online at: https://www.mayoclinic.org/diseases-conditions/mitral-valve-stenosis/symptoms-causes/syc-20353159 (Accessed May 29, 2024).

Mayo Clinic, Z. Z. (2025a). *Aortic Valve Stenosis - Symptoms and Causes*. Available online at: https://www.mayoclinic.org/diseases-conditions/aortic-stenosis/symptoms-causes/syc-20353139 (Accessed May 29, 2024).

Mayo Clinic, Z. Z. (2025b). *Heart Failure - Symptoms and Causes*. Available online at: https://www.mayoclinic.org/diseases-conditions/heart-failure/symptoms-causes/syc-20373142 (Accessed June 19, 2024).

Mazurek, T., Zhang, L., Zalewski, A., Mannion, J. D., Diehl, J. T., Arafat, H., et al. (2003). Human epicardial adipose tissue is a source of inflammatory mediators. *Circulation* 108, 2460–2466. doi: 10.1161/01.CIR.0000099542.57313.C5

Meenakshi, K., Rajendran, M., Srikumar, S., and Chidambaram, S. (2016). Epicardial fat thickness: a surrogate marker of coronary artery disease – assessment by echocardiography. *Indian Heart J*. 68, 336–341. doi: 10.1016/j.ihj.2015.08.005

Meloni, A., Frijia, F., Panetta, D., Degiorgi, G., De Gori, C., Maffei, E., et al. (2023). Photon-counting computed tomography (PCCT): technical background and cardio-vascular applications. *Diagnostics* 13:645. doi: 10.3390/diagnostics13040645

Menghoum, N., Badii, M. C., Leroy, M., Parra, M., Roy, C., Lejeune, S., et al. (2025). Exploring the impact of metabolic comorbidities on epicardial adipose tissue in heart failure with preserved ejection fraction. *Cardiovasc. Diabetol*. 24:134. doi: 10.1186/s12933-025-02688-7

Militello, C., Prinzi, F., Sollami, G., Rundo, L., La Grutta, L., Vitabile, S., et al. (2023). CT radiomic features and clinical biomarkers for predicting coronary artery disease. *Cogn. Comput*. 15, 238–253. doi: 10.1007/s12559-023-10118-7

Militello, C., Rundo, L., Toia, P., Conti, V., Russo, G., Filorizzo, C., et al. (2019). A semi-automatic approach for epicardial adipose tissue segmentation and quantification on cardiac CT scans. *Comput. Biol. Med*. 114:103424. doi: 10.1016/j.compbiomed.2019.103424

Miller, C. A., and Schmitt, M. (2011). Epicardial lipomatous hypertrophy mimicking pericardial effusion. *Circul. Cardiovasc. Imag*. 4, 77–78. doi: 10.1161/CIRCIMAGING.110.957498

MoosaviTayebi, R. (2014). *Echocardiography Image Segmentation: A Survey*. IEEE. Available online at: https://www.academia.edu/7479069/Echocardiography_Image_Segmentation_A_Survey (Accessed April 18, 2024).

Myerson, S. G., Roberts, R., Moat, N., and Pennell, D. J. (2004). Tamponade caused by cardiac lipomatous hypertrophy. *J. Cardiovasc. Magn. Reson*. 6, 565–568. doi: 10.1081/JCMR-120030585

Nabati, M., Salehi, A., Hatami, G., Dabirian, M., Yazdani, J., Parsaee, H., et al. (2019). Epicardial adipose tissue and its association with cardiovascular risk factors and mitral annular calcium deposits. *Ultrasound* 27, 217–224. doi: 10.1177/1742271X19846159

Nagashima, K., Okumura, Y., Watanabe, I., Nakai, T., Ohkubo, K., Kofune, T., et al. (2011). Association between epicardial adipose tissue volumes on 3-dimensional reconstructed CT images and recurrence of atrial fibrillation after catheter ablation. *Circ. J*. 75, 2559–2565. doi: 10.1253/circj.CJ-11-0554

Nakanishi, K., Fukuda, S., Tanaka, A., Otsuka, K., Sakamoto, M., Taguchi, H., et al. (2012). Peri-atrial epicardial adipose tissue is associated with new-onset nonvalvular atrial fibrillation. *Circ. J*. 76, 2748–2754. doi: 10.1253/circj.CJ-12-0637

Nerlekar, N., Baey, Y. W., Brown, A. J., Muthalaly, R. G., Dey, D., Tamarappoo, B., et al. (2018). Poor correlation, reproducibility, and agreement between volumetric versus linear epicardial adipose tissue measurement: a 3D computed tomography versus 2D echocardiography comparison. *JACC Cardiovasc. Imag*. 11, 1035–1036. doi: 10.1016/j.jcmg.2017.10.019

Nesti, L., Pugliese, N. R., Chiriacò, M., Trico, D., Baldi, S., Natali, A., et al. (2023). Epicardial adipose tissue thickness is associated with reduced peak oxygen consumption and systolic reserve in patients with type 2 diabetes and normal heart function. *Diabetes Obes. Metab*. 25, 177–188. doi: 10.1111/dom.14861

Norlén, A., Alvén, J., Molnar, D., Enqvist, O., Norrlund, R. R., Brandberg, J., et al. (2016). Automatic pericardium segmentation and quantification of epicardial fat from computed tomography angiography. *J. Med. Imag*. 3:034003. doi: 10.1117/1.JMI.3.3.034003

Painchaud, N., Duchateau, N., Bernard, O., and Jodoin, P. M. (2022). Echocardiography segmentation with enforced temporal consistency. *IEEE Trans. Med. Imag*. 41, 2867–2878. doi: 10.1109/TMI.2022.3173669

Parisi, V., Petraglia, L., Formisano, R., Caruso, A., Grimaldi, M. G., Bruzzese, D., et al. (2020). Validation of the echocardiographic assessment of epicardial adipose tissue thickness at the Rindfleisch fold for the prediction of coronary artery disease. *Nutr. Metab. Cardiovasc. Dis*. 30, 99–105. doi: 10.1016/j.numecd.2019.08.007

Patrick Lynch (2017). *My Medical Illustrations*. Available online at: https://coastfieldguides.com/my-medical-illustrations/ (Accessed July 8, 2024).

Pohost, G. M. (2008). The history of cardiovascular magnetic resonance. *JACC Cardiovasc. Imag*. 1, 672–678. doi: 10.1016/j.jcmg.2008.07.009

Priya, C., and Sudha, S. (2019). Adaptive fruitfly based modified region growing algorithm for cardiac fat segmentation using optimal neural network. *J. Med. Syst*. 43:104. doi: 10.1007/s10916-019-1227-3

Pugliese, N. R., Paneni, F., Mazzola, M., De Biase, N., Del Punta, L., Gargani, L., et al. (2021). Impact of epicardial adipose tissue on cardiovascular haemodynamics, metabolic profile, and prognosis in heart failure. *Eur. J. Heart Fail*. 23, 1858–1871. doi: 10.1002/ejhf.2337

Qi, Z., Wu, D., Yan, Z., Wang, Q., Li, Y., Zhao, J., et al. (2025). Role of epicardial adipose tissue in heart failure with preserved ejection fraction: an emerging molecular mechanism and therapeutic potential. *Obes. Rev*. 26:e13912. doi: 10.1111/obr.13912

Radswiki, T. (2025). *Radiopaedia. Cardiac lipoma*. Radiology Reference Article | Radiopaedia.org. Available online at: https://radiopaedia.org/articles/cardiac-lipoma?lang=us (Accessed May 29, 2024).

Requena-Ibáñez, J. A., Santos-Gallego, C. G., Rodriguez Cordero, A. J., Fardman, B., Sartori, S., Sanz, J., et al. (2022). Not only how much, but also how to, when measuring epicardial adipose tissue. *Magnetic Resonance Imag*. 86, 149–151. doi: 10.1016/j.mri.2021.11.004

Rhee, T. M., Lee, J. H., Choi, E. K., Han, K. D., Lee, H., Park, C. S., et al. (2017). Increased risk of atrial fibrillation and thromboembolism in patients with severe psoriasis: a nationwide population-based study. *Sci. Rep*. 7:9973. doi: 10.1038/s41598-017-10556-y

Rodrigues, É. O., de Morais, F. F. C., and Conci, A. (2022). On the automated segmentation of epicardial and mediastinal cardiac adipose tissues using classification algorithms. *arXiv*[Preprint] arXiv:2208.14352.

Rodrigues, É. O., Morais, F. F. C., Morais, N. A. O. S., Conci, L. S., Neto, L. V., Conci, A., et al. (2016). A novel approach for the automated segmentation and volume quantification of cardiac fats on computed tomography. *Comput. Methods Programs Biomed*. 123, 109–128. doi: 10.1016/j.cmpb.2015.09.017

Sacks, H., and Symonds, M. E. (2013). Anatomical locations of human brown adipose tissue: functional relevance and implications in obesity and type 2 diabetes. *Diabetes* 62, 1783–1790. doi: 10.2337/db12-1430

Salerno, M., Sharif, B., Arheden, H., Kumar, A., Axel, L., Li, D., et al. (2017). Recent advances in cardiovascular magnetic resonance: techniques and applications. *Circ. Cardiovasc. Imag*. 10:e003951. doi: 10.1161/CIRCIMAGING.116.003951

Schejbal, V. (1989). Epicardial fatty tissue of the right ventricle–morphology, morphometry and functional significance. *Pneumologie* 43, 490–499.

Schimmel, K., Ichimura, K., Reddy, S., Haddad, F., and Spiekerkoetter, E. (2022). Cardiac fibrosis in the pressure overloaded left and right ventricle as a therapeutic target. *Front. Cardiovasc. Med*. 9:886553. doi: 10.3389/fcvm.2022.886553

Schneider, M. P., Hua, T. A., Böhm, M., Wachtell, K., Kjeldsen, S. E., Schmieder, R. E., et al. (2010). Prevention of atrial fibrillation by Renin-Angiotensin system inhibition a meta-analysis. *J. Am. Coll. Cardiol*. 55, 2299–2307. doi: 10.1016/j.jacc.2010.01.043

Secchi, F., Asteria, C., Monti, C. B., Malavazos, A. E., Capra, D., Alì, M., et al. (2022). Quantification of epicardial adipose tissue in obese patients using an open-bore MR scanner. *Eur. Radiol. Exp*. 6:25. doi: 10.1186/s41747-022-00274-0

Si, Y., Feng, Z., Liu, Y., Fan, W., Shan, W., Zhang, Y., et al. (2023). Inflammatory biomarkers, angiogenesis and lymphangiogenesis in epicardial adipose tissue correlate with coronary artery disease. *Sci. Rep*. 13:2831. doi: 10.1038/s41598-023-30035-x

Sicari, R., Sironi, A. M., Petz, R., Frassi, F., Chubuchny, V., De Marchi, D., et al. (2011). Pericardial rather than epicardial fat is a cardiometabolic risk marker: an MRI vs echo study. *J. Am. Soc. Echocardiogr*. 24, 1156–1162. doi: 10.1016/j.echo.2011.06.013

Silaghi, A., Piercecchi-Marti, M. D., Grino, M., Leonetti, G., Alessi, M. C., Clement, K., et al. (2008). Epicardial adipose tissue extent: relationship with age, body fat distribution, and coronaropathy. *Obesity* 16, 2424–2430. doi: 10.1038/oby.2008.379

Song, Y., Tan, Y., Deng, M., Shan, W., Zheng, W., Zhang, B., et al. (2023). Epicardial adipose tissue, metabolic disorders, and cardiovascular diseases: recent advances classified by research methodologies. *MedComm* 4:e413. doi: 10.1002/mco2.413

Stanley, T. L., Feldpausch, M. N., Oh, J., Branch, K. L., Lee, H., Torriani, M., et al. (2014). Effect of tesamorelin on visceral fat and liver fat in HIV-infected patients with abdominal fat accumulation: a randomized clinical trial. *JAMA* 312:380. doi: 10.1001/jama.2014.8334

Stauffer, C. M., Meshida, K., Bernor, R. L., Granite, G. E., and Boaz, N. T. (2024). *Anatomy, Thorax, Pericardiacophrenic Vessels*. Treasure Island, FL: StatPearls Publishing. Available online at: http://www.ncbi.nlm.nih.gov/books/NBK559242/ (Accessed June 20, 2024).

Steenbergen, C., and Frangogiannis, N. G. (2012). "Chapter 36 - Ischemic heart disease," in *Muscle*, eds. J. A. Hill and E. N. Olson (Boston, Waltham, MA: Academic Press), 495–521. Available online at: https://www.sciencedirect.com/science/article/pii/B9780123815101000363 (Accessed June 18, 2024).

Tamarappoo, B., Dey, D., Shmilovich, H., Nakazato, R., Gransar, H., Cheng, V. Y., et al. (2010). Increased pericardial fat volume measured from noncontrast CT predicts myocardial ischemia by SPECT. *JACC Cardiovasc. Imag*. 3, 1104–1112. doi: 10.1016/j.jcmg.2010.07.014

Tran, K. V., Fitzgibbons, T., Min, S. Y., DeSouza, T., and Corvera, S. (2018). Distinct adipocyte progenitor cells are associated with regional phenotypes of perivascular aortic fat in mice. *Mol. Metab*. 9, 199–206. doi: 10.1016/j.molmet.2017.12.014

Tromp, J., Bryant, J. A., Jin, X., van Woerden, G., Asali, S., Yiying, H., et al. (2021). Epicardial fat in heart failure with reduced versus preserved ejection fraction. *Eur. J. Heart Fail*. 23, 835–838. doi: 10.1002/ejhf.2156

Tsao, H. M., Hu, W. C., Wu, M. H., Tai, C. T., Lin, Y. J., Chang, S. L., et al. (2011). Quantitative analysis of quantity and distribution of epicardial adipose tissue surrounding the left atrium in patients with atrial fibrillation and effect of recurrence after ablation. *Am. J. Cardiol*. 107, 1498–1503. doi: 10.1016/j.amjcard.2011.01.027

Vajihi, Z., Rosado-Mendez, I., Hall, T. J., and Rivaz, H. (2019). "L1 and L2 norm depth-regularized estimation of the acoustic attenuation and backscatter coefficients using dynamic programming," in *2019 IEEE 16th International Symposium on Biomedical Imaging (ISBI 2019)*, Venice Italy (IEEE), 1749–1752. Available online at: https://ieeexplore.ieee.org/document/8759099/ (Accessed July 13, 2023).

van Dam, A. D., Boon, M. R., Berbée, J. F. P., Rensen, P. C. N., and van Harmelen, V. (2017). Targeting white, brown and perivascular adipose tissue in atherosclerosis development. *Euro. J. Pharmacol*. 816, 82–92. doi: 10.1016/j.ejphar.2017.03.051

Van Woerden, G., Van Veldhuisen, D. J., Westenbrink, B. D., de Boer, R. A., Rienstra, M., and Gorter, T. M. (2022). Connecting epicardial adipose tissue and heart failure with preserved ejection fraction: mechanisms, management and modern perspectives. *Euro. J. Heart Fail*. 24, 2238–2250. doi: 10.1002/ejhf.2741

Virdis, A., Duranti, E., Rossi, C., Dell'Agnello, U., Santini, E., Anselmino, M., et al. (2015). Tumour necrosis factor-alpha participates on the endothelin-1/nitric oxide imbalance in small arteries from obese patients: role of perivascular adipose tissue. *Eur. Heart J*. 36, 784–794. doi: 10.1093/eurheartj/ehu072

Wang, Q., Chi, J., Wang, C., Yang, Y., Tian, R., Chen, X., et al. (2022). Epicardial adipose tissue in patients with coronary artery disease: a meta-analysis. *J. Cardiovasc. Dev. Dis*. 9:253. doi: 10.3390/jcdd9080253

Weerakkody, Y. (2021). *Radiopaedia. Epicardial Lipomatosis*. Radiology Reference Article | Radiopaedia.org. Available online at: https://radiopaedia.org/articles/epicardial-lipomatosis?lang=us (Accessed May 29, 2024).

Wen, D., An, R., Lin, S., Yang, W., Jia, Y., Zheng, M., et al. (2022). Influence of different segmentations on the diagnostic performance of pericoronary adipose tissue. *Front. Cardiovasc. Med*. 9:773524. doi: 10.3389/fcvm.2022.773524

Withers, S. B., Bussey, C. E., Saxton, S. N., Melrose, H. M., Watkins, A. E., Heagerty, A. M., et al. (2014). Mechanisms of adiponectin-associated perivascular function in vascular disease. *Arterioscler Thromb. Vasc. Biol*. 34, 1637–1642. doi: 10.1161/ATVBAHA.114.303031

Wu, C. K., Lee, J. K., Hsu, J. C., Su, M. Y. M., Wu, Y. F., Lin, T. T., et al. (2020). Myocardial adipose deposition and the development of heart failure with preserved ejection fraction. *Euro. J. Heart Fail*. 22, 445–454. doi: 10.1002/ejhf.1617

Wu, C. K., Tsai, H. Y., Su, M. Y. M., Wu, Y. F., Hwang, J. J., Lin, J. L., et al. (2017). Evolutional change in epicardial fat and its correlation with myocardial diffuse fibrosis in heart failure patients. *J. Clin. Lipidol*. 11, 1421–1431. doi: 10.1016/j.jacl.2017.08.018

Wu, F. Z., Huang, Y. L., Wang, Y. C., Lin, H. S., Chen, C. S., Ju, Y. J., et al. (2013). Impact of location of epicardial adipose tissue, measured by coronary artery calcium-scoring computed tomography on obstructive coronary artery disease. *Am. J. Cardiol*. 112, 943–949. doi: 10.1016/j.amjcard.2013.05.022

Xiao, J., Lu, Y., and Yang, X. (2020). Ultrasound detection of epicardial adipose tissue combined with ischemic modified albumin in the diagnosis of coronary heart disease. *Heart Surg. Forum* 23, E461–E464. doi: 10.1532/hsf.3015

Xu, Y., Hrybouski, S., Paterson, D. I., Li, Z., Lan, Y., Luo, L., et al. (2022). Comparison of epicardial adipose tissue volume quantification between ECG-gated cardiac and non-ECG-gated chest computed tomography scans. *BMC Cardiovasc. Disord*. 22:545. doi: 10.1186/s12872-022-02958-2

Yamaguchi, Y., Cavallero, S., Patterson, M., Shen, H., Xu, J., Kumar, S. R., et al. (2015). Adipogenesis and epicardial adipose tissue: a novel fate of the epicardium induced by mesenchymal transformation and PPARγ activation. *Proc. Natl. Acad. Sci. U.S.A*. 112, 2070–2075. doi: 10.1073/pnas.1417232112

Yin, L., Yan, C., Yang, C., Dong, H., Xu, S., Li, C., et al. (2022). Measurement of epicardial adipose tissue using non-contrast routine chest-CT: a consideration of threshold adjustment for fatty attenuation. *BMC Med. Imag*. 22:114. doi: 10.1186/s12880-022-00840-3

Zhang, P., Konja, D., and Wang, Y. (2020). Adipose tissue secretory profile and cardiometabolic risk in obesity. *Endocrine Metabolic Sci*. 1:100061. doi: 10.1016/j.endmts.2020.100061

Zhang, Q., Zhou, J., Zhang, B., Jia, W., and Wu, E. (2020). Automatic epicardial fat segmentation and quantification of CT scans using dual U-nets with a morphological processing layer. *IEEE Access*. 8, 128032–128041. doi: 10.1109/ACCESS.2020.3008190

Zhou, M., Wang, H., Chen, J., and Zhao, L. (2020). Epicardial adipose tissue and atrial fibrillation: possible mechanisms, potential therapies, and future directions. *Pacing Clin. Electrophysiol*. 43, 133–145. doi: 10.1111/pace.13825

Zyuzin, V., Mukhtarov, A., Neustroev, D., and Chumarnaya, T. (2020). "Segmentation of 2D echocardiography images using residual blocks in U-net architectures," in *2020 Ural Symposium on Biomedical Engineering, Radioelectronics and Information Technology (USBEREIT)* (Yekaterinburg: IEEE), 499–502. doi: 10.1109/USBEREIT48449.2020.9117678